AD-A150 167 ELECTRICAL AND THERMAL TRANSPORT PROPERTY STUDIES OF HIGH-TEMPERATURE THE.. (U) BATTELLE PACIFIC NORTHWEST LAB RICHLAND WA J L BATES ET AL. JUL 84 1/2

UNCLASSIFIED AFOSR-TR-84-1210 F49620-83-C-0109 F/G 11/2 NL

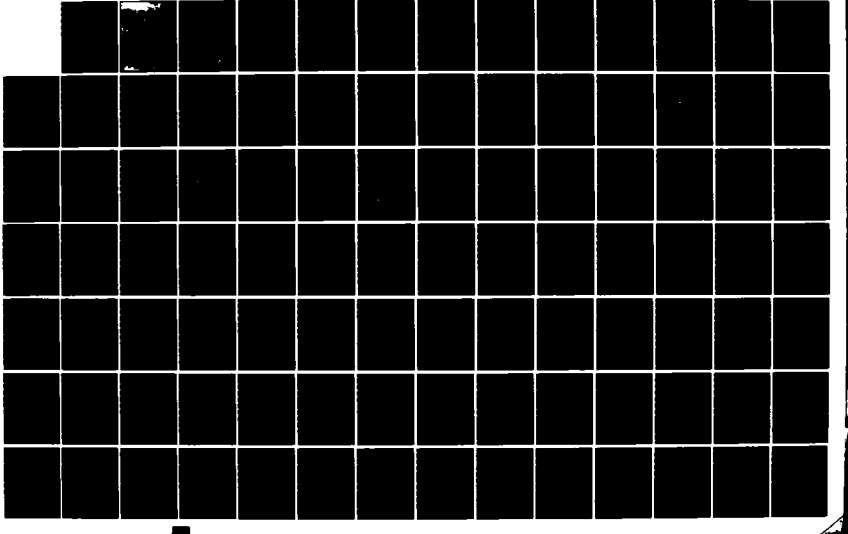

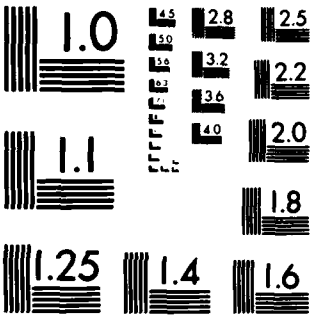

ELECTRICAL AND THERMAL TRANSPORT PROPERTY STUDIES OF HIGH-TEMPERATURE THERMOELECTRIC MATERIALS: INTERIM TECHNICAL REPORT FOR THE PERIOD AUGUST 15, 1983 to MAY 15, 1984

J. L. Bates
J. E. Garnier
L. C. Olsen*
C. W. Griffin

Battelle
Pacific Northwest Laboratories

(3)

ELECTRICAL AND THERMAL TRANSPORT PROPERTY STUDIES OF HIGH-TEMPERATURE THERMOELECTRIC MATERIALS: INTERIM TECHNICAL REPORT FOR THE PERIOD AUGUST 15, 1983 to MAY 15, 1984

J. L. Bates
J. E. Garnier
L. C. Olsen*
C. W. Griffin

July 1984

Prepared for

Air Force Office of Scientific Research
under AFOSR Contract F49620-83-C0109

Battelle, Pacific Northwest Laboratories
Richland, Washington 99352

* Consultant

CONTENTS

CONTENTS

FIGURES

FIGURES (Cont.)

TABLES

1.0 SUMMARY

The first year of this research has emphasized the study of electronically conducting oxides with varied transport characteristics, an evaluation of theoretical models, and the determination of a high-temperature transport property data base. Oxide systems based on SnO_2-In_2O_3, (La,Y)(Mg,Ca,Sr)CrO_3, HfO_2-R_xO_y-In_2O_3 and La(Sr)MnO_3 were selected for initial studies and represent different crystallographic/defect structures and transport characteristics. The electrical conductivity, Seebeck coefficient and thermal conductivity for these oxides are being measured and have provided a preliminary data base for evaluating transport properties and the figure of merit. This includes the development of a novel technique for the rapid, high-temperature determination of the absolute Seebeck coefficient.

Theories for the figure of merit, the transport properties of broad- and narrow-band semiconductors with emphasis on small polaron or hopping conduction were developed and applied to SnO_2-In_2O_3, Y(M)CrO_3 and La(Sr)MnO_3. The highly conducting SnO_2-In_2O_3 are degenerate, n-type broad-band semiconductors with low Seebeck coefficients and small figures of merit. The (Y)(Ca,Mg,Sr)CrO_3 are p-type, narrow-band semiconductors with low thermal conductivities, high Seebeck coefficients and moderate electrical conductivity. These ABO_3 oxides are of the controlled valency type and, by varying the divalent or trivalent substitutions on either the A and B sites, have the potential for altering the transport properties for optimum high figure of merit.

Current research emphasizes small polaron transport in narrow-band semiconducting oxides. The predicted and measured increases in both the Seebeck coefficient and electrical conductivity with increasing temperature makes them exciting as high-temperature thermoelectric materials with potential to increase the figure of merit. Future research will emphasize these types of highly conducting materials and include the rare-earth chromites, chalcogenides and oxy-chalcogenides.

2.0 INTRODUCTION

The purpose of this report is to describe the technical results obtained during the first year's study of high-temperature thermoelectric materials.[(a)] The scope of the research is: a) to develop theoretical models for electrical, thermal, and thermoelectric behavior of refractory oxide materials, b) to determine electrical transport properties necessary to develop and test these models, c) to determine methods for increasing the figure of merit in refractory oxide systems by varying composition, defect structure, microstructure, etc., and d) to use these models to establish theoretical and empirical limits of the figure of merit for these oxides and other refractory materials.

The general approach for evaluating the figure of merit, (ZT),

$$ZT = \frac{\sigma S^2}{\lambda} T$$

is to study thermally stable materials such as refractory oxides, sulfides, oxysulfides, and other chalcogenides that generally exhibit low thermal conductivities (λ), <10 W/m-K, but with moderate electrical conduction (σ), >10 ohm^{-1}-cm^{-1}, and high Seebeck coefficients (S), >200 μV/K. It is the intent of this program to investigate a number of oxide and oxysulfide systems that exhibit these properties.

The emphasis this first year was: 1) to complete a literature review of potential refractory oxides that should be considered for study and to select those that might best represent different crystallographic or defect structures with different transport characteristics, 2) to initiate transport and thermal property measurements to provide a data base for evaluating possible models for high-temperature thermoelectric refractory materials, and 3) to consider these data using present theories for thermoelectric conversion and electrical transport in broad- and narrow-band semiconductors.

(a) This covers the period from August 15, 1983, to May 15, 1984. The abbreviated year resulted from a 3-month delay in receipt of the signed contract.

The literature review and evaluation, the transport property measurement techniques and data for selected oxide systems, the theoretical considerations for high-temperature thermoelectric materials with ZT >1, conclusions and future research are described in the body of this report. The refractory materials initially studied and reported include the $(Y)(M)CrO_3$, SnO_2-In_2O_3, $HfO_2(ZrO_2)$-R_xO_y-In_2O_3, and $La(M)MnO_3$. In addition, appended to this report are the tabulation of data and the draft of a paper being prepared for publication.

3.0 OTHER THERMOELECTRIC MATERIALS WORK

Current advanced research efforts on thermoelectric materials are concentrating on the development of materials for high-temperature applications. In particular, materials with a dimensionless figure of merit (ZT) greater than 1 for temperatures above 1000 K are of primary interest. Research and development efforts conducted from 1950 to 1980 led to several materials with ZT of about 1 in the temperature range of 300 K to 1200 K. These materials are briefly discussed below. Research on high-temperature thermoelectric materials by other groups presently involves two classes of materials: rare-earth chalcogenides and boron-rich borides. These compounds are also briefly discussed in this section.

3.1 PREVIOUSLY DEVELOPED MATERIALS

During the 1950's and 1960's, the theory for thermoelectric materials based on broad-band semiconductors was well developed. This work resulted in the following basic approach for thermoelectric materials development:

* Select compounds for development so that the lattice component of thermal conductivity can be minimized:
* Select semiconducting materials for which the dopant concentration can be adjusted to achieve maximum σS^2.

By 1980, several useful n- and p-type thermoelectric materials had been developed. Plots of ZT versus T for some of these materials are given in Figure 3.1. Note that these materials collectively spans the temperature range of 300 K to 1200 K. The need for thermoelectric materials with large values of ZT above 1300 K is evident. It is particularly desirable to have thermoelements that exhibit a ZT of 1 or greater over a large temperature interval up to 2000 K. Such an achievement may require thermoelements with graded composition profiles. However, material systems capable of efficient thermoelectric power generation at high temperatures must be first identified and developed.

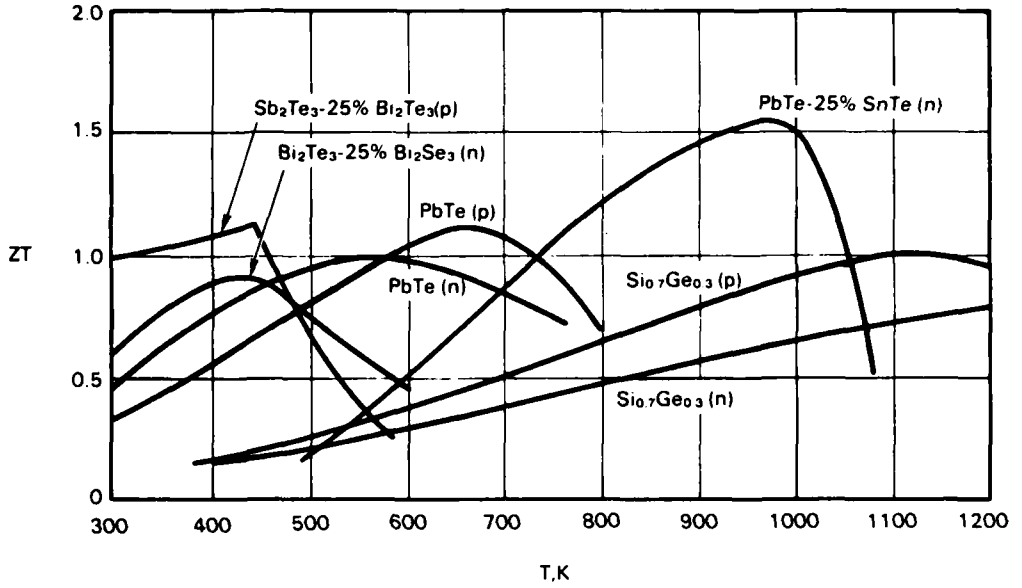

FIGURE 3.1. Dimensionless Figures of Merit for Thermoelectric Materials. Developed by 1980.

3.2 RARE-EARTH CHALCOGENIDES

The rare-earth chalcogenides form three binary compounds: RX, R_3X_4-R_2X_3, and RX_2. R refers to a rare-earth atom, while X refers to a chalcogen (S, Se, or Te). The R_3X_4-R_2X_3 compounds are being investigated for thermoelectric energy conversion.[3.1, 3.2, 3.3] In the case of R_3X_4, there are no vacant sites; while in R_2X_3, a significant number of rare-earth sites are empty. These vacancies apparently act as donors, and the materials are heavily doped.

The rare-earth sulfides are n-type, broad-band semiconductors. Due to the large doping level, they usually are degenerate. Electrical transport properties can be interpreted as being a result of electrons moving in a conduction band with effective masses several times the free electron mass. Thus, an itinerant model for electron transport is adequate for the rare-earth chalcogenides.

The lattice component of thermal conductivity for these materials is relatively low because of the rather complex structure. There are 28 atoms

per unit cell and there is usually a high density of vacancies. Figure 3.2 summarizes ZT versus T data for some of these materials. These results are encouraging. But there is still a need for materials with ZT >1 at high temperatures.

3.3 BORON-RICH BORIDES

Boron forms a large number of refractory compounds. Four borides have been investigated for high-temperature thermoelectrics: β-boron, $B_{14}Si$, B_xC, and α-AlB_{12}.[3.1, 3.4, 3.5] These compounds all have a large number of atoms per unit cell. Figure 3.3 shows results for ZT versus T.

These materials are all p-type. The Seebeck coefficient and electrical conductivity both increase with temperature over a relatively large temperature interval. The electrical transport properties of the borides have been interpreted in terms of small polarons hopping between inequivalent sites. The structures of these borides are compatible with such a concept.

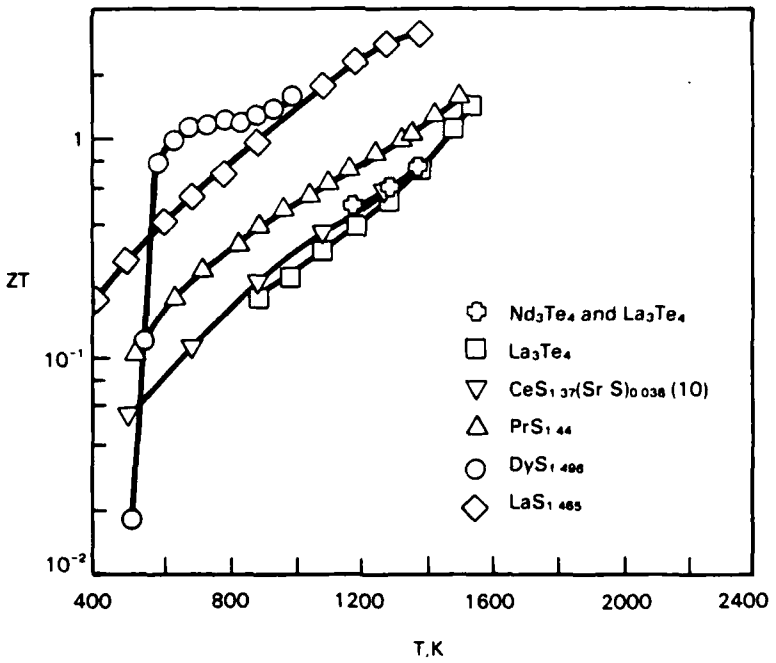

FIGURE 3.2. ZT Values for Rare-Earth Chalcogenides.[3.1]

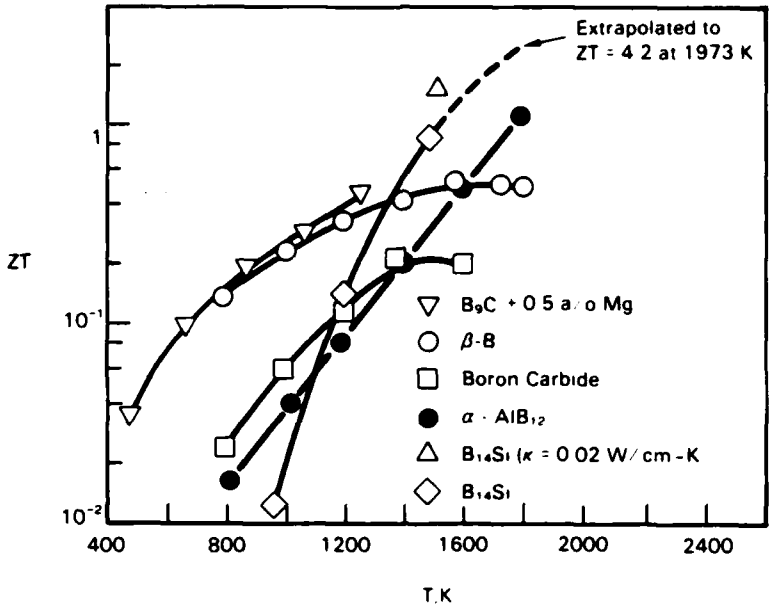

FIGURE 3.3. Values for Boron and Boron-Rich Borides[3.1]

A significant part of the current research activities on the borides is devoted to studies of small polaron transport. Theoretical studies of the figure of merit of such materials are needed. Thus, the work being done on this program should be beneficial to workers investigating the borides.

4.0 THEORETICAL STUDIES

In this section, the theory for thermoelectric energy conversion and the theories for electrical transport in broad-band and narrow-band semiconductors are reviewed. The concept of a figure of merit is introduced. Potential values for the figure of merit of each type of semiconductor are considered. Heike and Ure[4.1] discuss thermoelectric theory in greater detail.

4.1 BRIEF REVIEW OF THERMOELECTRIC ENERGY CONVERSION

Consider a simple thermocouple as shown in Figure 4-1. Heat (Q) is being absorbed at the hot junction (T_H) and rejected at the cold junction

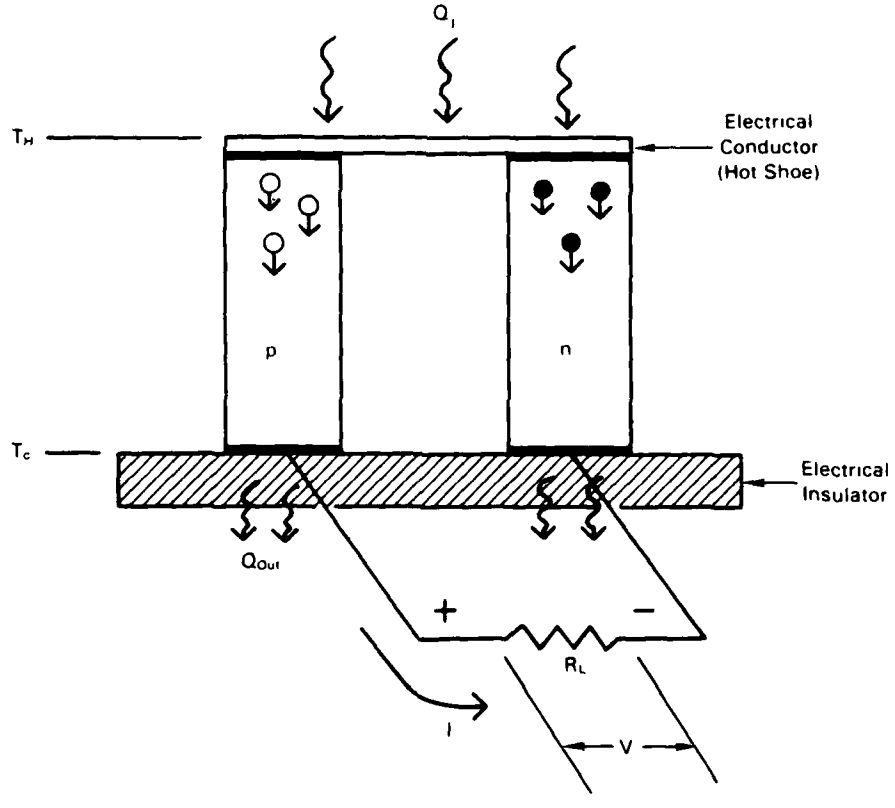

Figure 4.1. Schematic Illustration of Thermoelectric Converter Consisting of One n-Type and One p-Type Thermoelement.

(T_C) such that a temperature difference is established across the thermocouple. As a result of the temperature difference, carriers essentially undergo thermal diffusion. Electrons in the n-type material are driven from the "hot" to "cold" ends of the n-thermoelement, and holes in the p-type material are driven from the "hot" to "cold" ends of the p-thermoelement. The flow of electrons and holes gives rise to a current (I) through the load (R_L). In order to determine an expression for efficiency of this simple power source, one needs an expression for (I) as a function of the load voltage (V).

By considering both thermal diffusion and effects of an electric field on electrons and holes, one can show that at an interface within the p-type or n-type elements, and normal to the current flow, the current density is given by

$$J = \sigma[E_o - S \frac{dT}{dx}]$$

where σ is the material electrical conductivity, E_o is the electric field, and dT/dx is the thermal gradient at the interface. Consider a line integral of E_o around the circuit:

$$\oint E_o dx = o = \oint (\frac{J}{\sigma} + S \frac{dT}{dx}) dx$$

$$R\ I = \int_{T_c}^{T_H} S_p dT - \int_{T_c}^{T_H} S_n dt$$

$$= \int_{T_c}^{T_H} (S_p + |S_n|) dT$$

This result is an example of Kirchoff's voltage law, namely, the sum of emf's equals the sum of potential drops around a circuit. The term involving the Seebeck coefficient (S) is an electromotive force due to

thermal diffusion. If there are more than one n- and p-type thermoelements connected series with several resistive loads, one can write

$$\sum_i R_i I = \sum_{n-p} \int_{T_c}^{T_H} (S_p + |S_n|) dT$$

Assuming one load resistance, R_L, the output power can be written as $R_L I^2$. To calculate efficiency, an expression for the heat absorbed by the system is required. Transport theory leads to

$$Q_i = K_{T_H} \Delta T + (\pi_{pn})_{T_H} I - \tfrac{1}{2} R_I I^2$$

where

$$K = \lambda_n \left(\frac{A_n}{L_n}\right) + \lambda_p \left(\frac{A_p}{L_p}\right)$$

$$R_I = \rho_n \left(\frac{L_n}{A_n}\right) + \rho_p \left(\frac{A_p}{L_p}\right)$$

$$(\pi_{pn})_{T_H} = (S_p + |S_n|) T_H$$

There are three types of terms in the expression for Q_i, namely: heat transfer; Peltier effects; and Joule heating. The heat transfer terms simply involve thermal conduction along the thermoelements. Thus, the elements' thermal conductivities and aspect ratios are important parameters. The term involving π_{pn} refers to heat absorption, as described by Figure 4-2. The third term is due to Joule heating. Basically, one-half of the Joule heating in each element returns to the hot junction.

The efficiency of the system is

$$\eta = \frac{R_L I^2}{Q_i}$$

It can be written as

$$I = (R_I + R_L)^{-1} \int_{T_c}^{T_H} (S_p + |S_n|)dT$$

$$= \frac{S\,T}{R_I + R_L}$$

where $S = S_p + |S_n|$ and R_I is the internal resistance. S_n and S_p are assumed to be constant with temperature. Using the above expressions for I and Q_i,

$$\eta = \frac{R_L\, S^2(\Delta T)^2\, (R_L + R_I)^{-2}}{K\Delta T + ST_H I - \tfrac{1}{2} R_I S^2 \Delta T^2}$$

The expression for efficiency can be written as

$$\eta = \left[\frac{M}{\frac{(1+M)^2}{T_H} \frac{R_I K}{S^2} + (1+M) - \frac{\frac{1}{2}\Delta T}{T_H}} \right] \frac{\Delta T}{T_H}$$

where

$$M = R_L/R_I.$$

Assuming T_H and T_c are fixed, there are two quantities which can be varied, $R_I K$ and M. The expression for efficiency can be maximized by first determining values of parameters which minimize the product $R_I K$, and then,

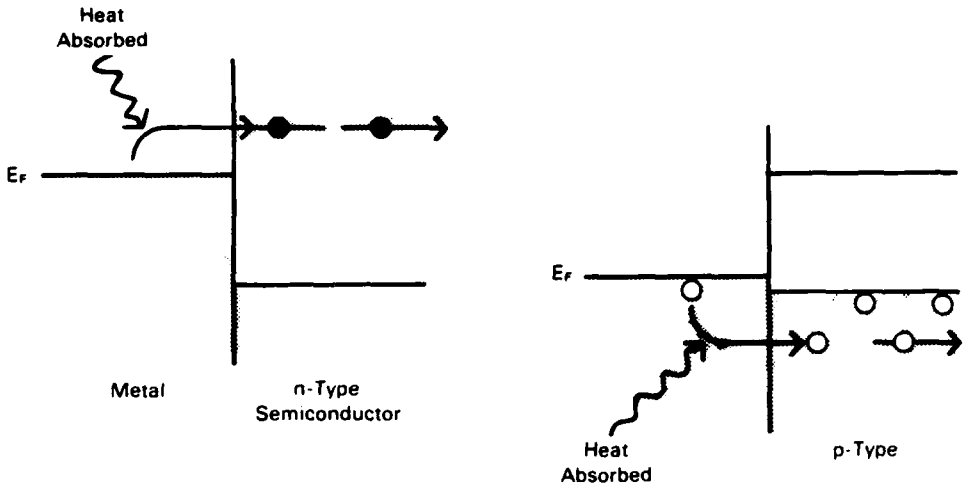

FIGURE 4.2. Peltier Effects at Hot Junction. Heat is absorbed at junction by electrons and holes entering the n-type and p-type thermoelectrics.

by finding the optimum value of M, for which η is maximized. After taking these steps, one finds that the maximum efficiency is given by

$$\eta_{MAX} = \frac{M_o - I}{M_o + (T_c/T_H)} \quad \frac{\Delta T}{T_H}$$

where

$$M_o = \begin{bmatrix} \text{OPTIMUM} \\ \text{VALUE OF} \\ \text{M} \end{bmatrix} = (1 + Z^* \bar{T})^{\frac{1}{2}}$$

$$Z^* = \frac{(S_n + S_p)^2}{[(\rho_n \lambda_n)^{\frac{1}{2}} + (\rho_p \lambda_p)^{\frac{1}{2}}]^2}$$

and

$$\frac{(A_n)}{L_n} (\sigma_n \lambda_n)^{\frac{1}{2}} = \frac{(A_p)}{L_p} (\sigma_p \lambda_p)^{\frac{1}{2}}$$

$$(RK)_{MIN} = [(\rho_n \lambda_n)^{\frac{1}{2}} + (\rho_p \lambda_p)^{\frac{1}{2}}]^2$$

One usually uses temperature-averaged transport parameters for each n- and p-type material in calculations of power source performance. It is often

convenient, however, to assume the n- and p-type materials to have the same values for S, σ and λ. Then,

$$Z^* = Z = \frac{\sigma S^2}{\lambda}$$

The product ZT is dimensionless and has a value on the order of one for efficient materials.

Figure 4.3 shows the efficiency of a single-stage thermoelectric generator, which operates between 300 K and the indicated value of T_H, and for which the thermoelectric elements are assumed to have constant values of ZT from 300°K to T_H. For efficiencies greater than 10%, one must use thermoelectric materials with ZT $\cong$ 1 over a ΔT = 300 K.

Thermoelectric generators based on two or more stages of thermoelectric material are clearly of interest for high efficiencies. A particular thermoelectric material will have ZT $\cong$ 1 only for $\Delta T \cong$ 200 K to

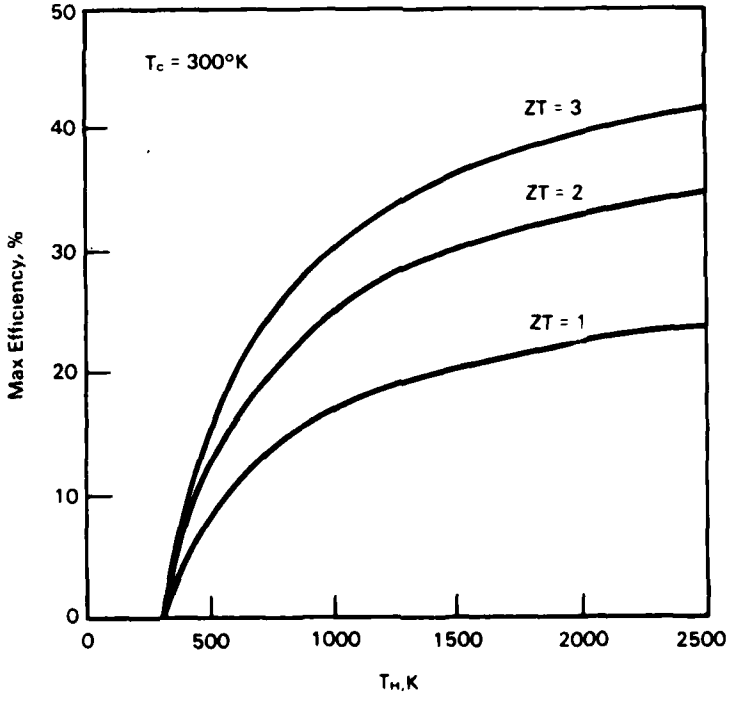

FIGURE 4.3. Calculated Maximum Efficiency Versus T_H for T_c = 300 K

400 K. To construct systems operating over much larger values of ΔT (and larger Carnot efficiencies), it is necessary to consider cascaded systems. One approach to this problem may involve the use of thermoelements with graded composition. Complex oxides, such as those materials considered in this program, may be particularly suited to such an approach.

4.2 THEORY FOR MATERIAL FIGURE OF MERIT

The figure of merit (ZT) as defined in the previous section, indicates the practical value of a material if used in a thermoelectric generator. Theory of semiconductors allows one to go further in identifying desirable materials for thermoelectric energy conversion. The transport properties, S, σ and λ can be expressed in terms of more basic material properties. In particular, the figure of merit can be written in terms of Fermi level, carrier-effective mass, scattering parameters, etc. It is convenient to discuss theory for the figure of merit for two kinds of semiconducting materials, namely, broad-band and narrow-band semiconductors.

4.2.1 Broad-Band Semiconductors

The term "broad band" refers to the width of an electron band. Referring to Figure 4-4, E_v is the width of the valence band. Electron states in

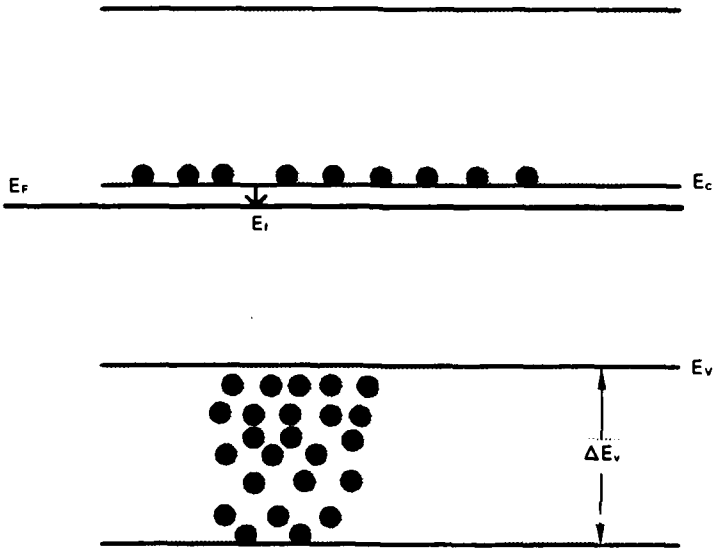

FIGURE 4.4. Electron Band Diagram for n-Type, Broad-Band Semiconductor.

such cases are characterized by extended wave functions. Transport of electrons in such bands can be described by particles moving through the crystal with an effective mass. The discussion here will refer to an n-type semiconductor, as described in Figure 4.4. Similar results are obtained for a p-type material.

Transport theory leads to the following results for σ, S and λ:

$$\sigma = ne\mu$$

$$S = \left(\frac{k}{e}\right)\left[\frac{E_f}{kT} + \left(r + \frac{5}{2}\right)\right]$$

$$\lambda = \lambda_\ell + \lambda_e = \lambda_\ell + L\sigma T$$

where

$$n = \frac{2}{\pi^{\frac{1}{2}}} N_c F_{\frac{1}{2}}(E_f/kT) \qquad N_c = 2.5 \times 10^{19}\ cm^{-3}$$

r = Electron scattering parameter

λ_ℓ = Lattice component of thermal conductivity

$\lambda_e = L\sigma T$ = Electron component of thermal conductivity

$L = \left(r + \frac{5}{2}\right)\left(\frac{k}{e}\right)^2$

k = Boltzmann's constant

e = Absolute value of electron charge

k/e = 86.3 μV/K

$F_{\frac{1}{2}}(x)$ = Fermi-Dirac integral

The dimensionless figure-of-merit can be written as

$$ZT = \frac{A\left(\varepsilon_f + r + \frac{5}{2}\right)^2 F_{\frac{1}{2}}(\varepsilon_f)}{\pi^{\frac{1}{2}} + \left(r + \frac{5}{2}\right) A\, F_{\frac{1}{2}}(\varepsilon_f)}$$

where

$$A = \left(\frac{k}{e}\right)^2 \frac{N_c\, e\mu T}{\lambda_\ell}$$

$$\varepsilon_f = \frac{E_f}{kT}$$

The parameter A is dimensionless. In fact, it is basically ZT for a case where $S = (k/e) = 86.3\ \mu V/K$, $\sigma = N_c e \mu$ and $\lambda = \lambda_\ell$ (i.e., λ is due only to lattice conduction).

Figure 4-5 shows results for ZT versus ε_f for various values of A. The optimum values for ε_f are indicated. The scattering parameter (r) has been set equal to -1/2, which corresponds to electron transport being limited by lattice scattering. The maximum value of ZT for a given material depends on the material parameter A. To obtain the maximum value of ZT, the optimum dopant concentration must be achieved. If the material is n-type, then the required donor density N_d is determined by setting $N_d = n$, where n is determined by ε_f.

A key question for thermoelectric material research concerns the maximum value of ZT. To address this question, one can simply investigate the possible value of A. Ure has addressed this question.[4.2] He considered a large body data for thermoelectric materials. Ure concluded that if $\lambda_\ell = 0.004$ W/cm K, then ZT values on the order of 3 to 4 appear possible.

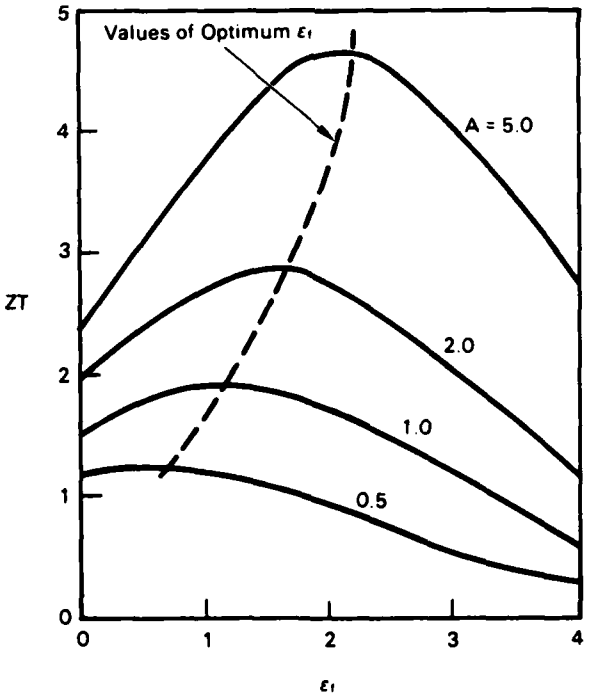

FIGURE 4.5. Calculated ZT versus ε_F for Values of the Material Parameter A, and for Lattice Scattering (r = -1/2).

Thermoelectric materials based on rare-earth chalcogenides are one class of materials currently being investigated as potential high-temperature materials. Some of these compounds have exhibited values of ZT > 1. These materials can be described by the broad-band model presented in this section. Further efforts may lead to ZT values suggested by Ure.

4.2.2 Narrow-Band Semiconductors

Another class of semiconductors which is also important to thermoelectrics consists of semiconductors with narrow bands. In these materials, the outer electrons of the constituent atoms are more localized. As a result, only a narrow band of energy forms. The band width is directly related to the amount of electron overlap. In the limit of widely-separated atoms, the band corresponding to atomic orbitals reduces to essentially the energy level width.

Electrons or holes in narrow bands move through solids, either by tunneling through a potential well, or by hopping. Above room temperature, the hopping transport mechanism is dominant. Hopping mobilities are usually low, 0.1 to 10 cm^2/V-sec. The carrier density is often quite large, however. As a result, the electrical conductivity can be as large in narrow-band materials as broad-band materials.

A detailed theory of the material figure of merit for narrow band materials has not been developed. However, each of the transport properties can be expressed in terms of key parameters. The hopping transport mechanism is usually by small polaron transport. Figure 4-6 illustrates the physical nature of small polarons, and an electron-band diagram useful for discussing small polaron transport. A small polaron refers to an electron and the polarized lattice around the electron. First, suppose that an electron is placed on an outer electron level (say 3d orbital of a transition metal atom), as indicated by the shaded area in Figures 4.6A. Since the electron is concentrated at a particular site, the surrounding positive ions are attracted toward the negative charge. As a result, instead of the electron being on a level at E_c, it is effectively at a level E_b below the conduction band edge. In order for the electron to move, it must receive energy from the lattice so that it can first undergo a transition to E_c and then move to another lattice site. This process is thermally activated and is referred to as hopping.

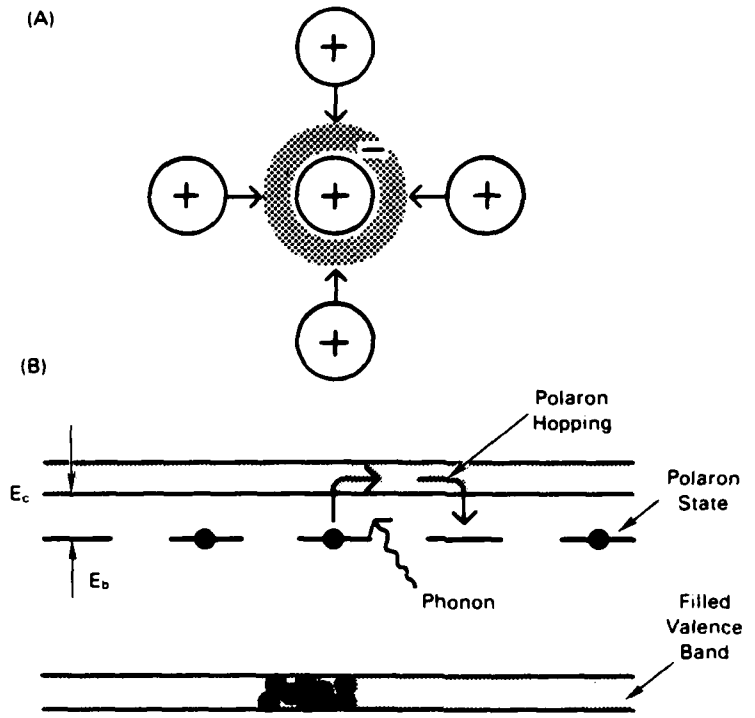

FIGURE 4.6. (A) Physical Description of Small Polaron.
(B) Electron Band Diagram Showing Polaron Transitions Involved in Polaron Transport.

The mobility of small polarons is given by

$$\mu = \frac{e\nu}{kT} \; a^2 \exp\left(\frac{-E_b}{kT}\right)$$

where ν is the characteristic frequency for high-frequency lattice vibrations, "a" is the intersite distance for hopping. The density of small polarons is usually fairly constant with temperature. Thus, the conductivity is given by(3.1)

$$\sigma = ne\mu$$

$$= \frac{N_o e\nu}{kT} \; a^2 \exp\left(-E_b/kT\right) = C_c \, T^{-1} \exp\left(-E_b/kT\right)$$

Usually σ increases slowly with temperature. More importantly, it continues to increase even at very large temperatures.

The Seebeck coefficient is given by[3.1]

$$S = A + BT$$

where

$$A = \frac{k}{e} \ln\left[\frac{2(1-c)}{c}\right]$$

$$B = \left(\frac{k}{e}\right) \frac{z J^2}{2 E_b^3}$$

where

c = Fraction of sites occupied by a carrier

z = Number of nearest neighbors

J = Intersite transfer energy in hopping process

E_b = Binding energy of polaron.

A is usually constant. B is finite only if hopping occurs between inequivalent sites. Thus, J = 0 for hopping between identical sites. If J≠0, then S increases with temperature. The behavior of S for small polaron materials makes these materials potentially exciting for thermoelectric applications. The borides, discussed previously, are an example of such a material. Other narrow-band materials which appear interesting to study are the perovskites, e.g., chromites. Preliminary results for these materials are discussed in this report.

Combining S, λ, and σ for small polaron materials to obtain estimates for ZT needs to be done. Earlier work by Ure resulted in estimates for possible ZT values for mixed-valence oxides to be on the order of 0.1 to 1. He did not include the BT term, however, Thus, a key objective of future work will be to carry out theoretical studies to estimate ZT for narrow-band materials.

5.0 TRANSPORT PROPERTY MEASUREMENTS

Accurate transport property data are required for understanding and developing theories and models for thermoelectric materials. These data must be generated over a wide temperature range for each material structure and composition as a function of atmosphere. The methods used to measure the thermal conductivity, electrical conductivity, transference numbers, and Seebeck coefficient are described. The technique for determining the Seebeck coefficient is described in more detail since a novel method was developed for measuring accurate, absolute values of S at temperatures up to 1600 K.

5.1 ELECTRICAL CONDUCTIVITY (σ)

The electrical conductivity is determined using a four-contact method, Figure 5.1. Rectangular bars nominally 3.8-cm long and 3-mm square were positioned in a resistance-heated, Al_2O_3 muffle furnace with platinum hardware. The direct currents and voltages are measured in both directions using a digital voltmeter and a digital microampmeter, accurate to ±1%. The emf is determined at each temperature and accounted for in calculating the sample resistance. The coefficients of determination are generally better than 0.98 at high temperatures and 0.95 at lower temperatures. Measurements are made both on heating and cooling from room temperature to 1650 K. The accuracy of the measurement is to within ±1%.

The data are fitted to both linear log σ versus K^{-1} and log σK versus K^{-1} relationships. The fitted data are used to calculate the figure of merit.

5.2 THERMAL CONDUCTIVITY (λ)

The thermal conductivity is determined from the product of the thermal diffusivity, specific heat, and density. The thermal diffusivity (α) is measured using the flash or pulse technique.[5.1-5.6] This method consists of heating one surface of a thin sample disc with a short pulse from a ruby laser. The heat passes through the sample and the temperature transient on

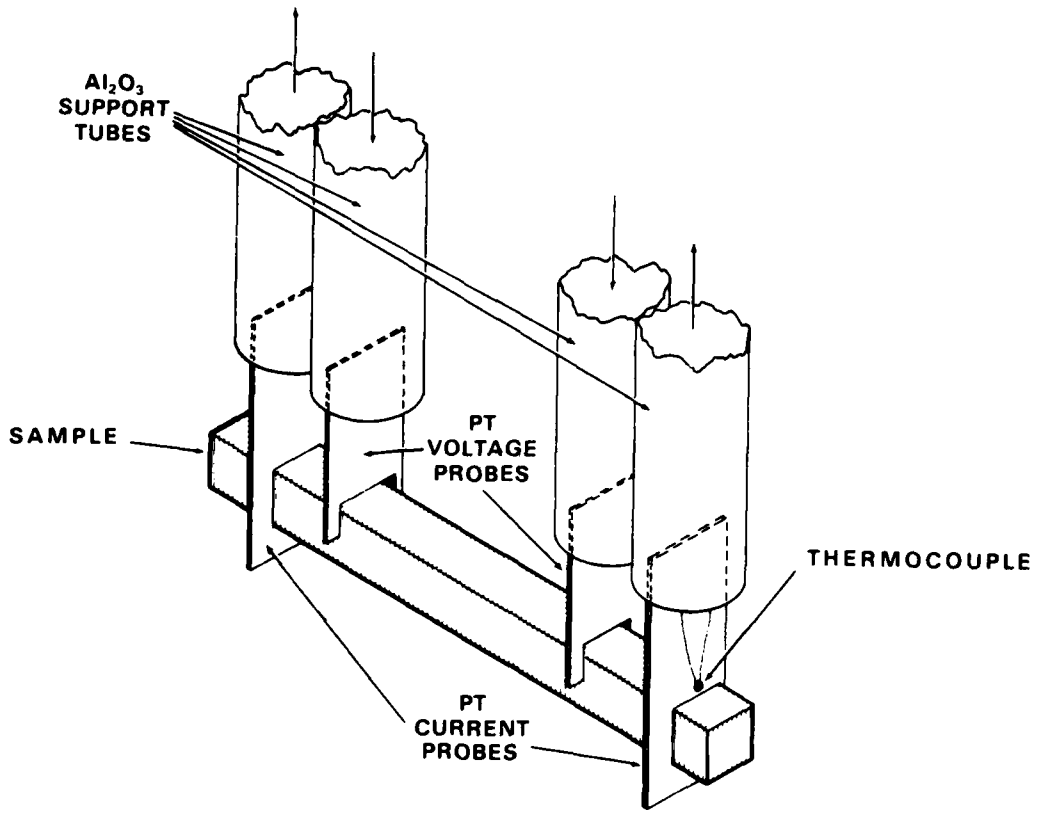

FIGURE 5.1. Four-Contact Method Used to Measure Electrical Conductivity

the back surface is measured with an optical detector. The temperature changes with times are recorded and α is determined from the shape of the curve.

The samples were heated in a tungsten resistance furnace inside a water-cooled, copper jacket. The samples were supported in a sintered Al_2O_3 holder which was positioned in a tungsten tube inside the furnace cavity. A thermocouple was inserted inside the sample holder to measure the ambient temperature. The temperature of the furnace was raised in steps from 50 to 200 degrees with measurements made both on heating and cooling at each temperature step. Measurements were made in purified argon at a slightly positive pressure.

The heat pulse was provided with a 10 to 15 Joule ruby laser with a pulse time of 0.0014 seconds. The temperature on the back surface was measured with a liquid nitrogen-cooled, InSb, infrared detector.

The time-temperature data were input into a transient waveform recorder. The digital form of the curve was recorded on magnetic tape and

fed into a computer programmed to correct for heat losses and to calculate the thermal diffusivity. The thermal conductivity was calculated from the thermal diffusivity and specific heat, density, and thermal expansion data provided to the program.

The conductivity data were fitted to a λ^{-1} versus K or polynomial curve. The fitted data were used to calculate the figure of merit.

The specific heat used for the calculation was obtained from: 1) reported literature values; 2) calculated values using the Kopp-Neumann relationship where the C_p of a mixed component is equal to the sum of the product of the individual compound constituents, and/or, 3) measured heat capacities up to 1175 K using a differential scanning calorimeter (DSC) with higher temperature values calculated from an extrapolation of the DSC data, using the Kopp-Neumann expression for the same or like compounds. This value was verified using Debye's expression for C_p at high temperatures.

The density was measured at room temperature, ρ_o, and corrected for temperature using measured thermal expansion values

$$\rho = \rho_o(1 + 3\Delta L/L)^{-1}$$

The precision and accuracy of the thermal conductivity data are within ±5% and represent the largest error in calculating the figure of merit.

5.3 SEEBECK COEFFICIENT

A novel experimental apparatus was developed for determining the Seebeck coefficient of potential thermoelectric materials and is described briefly in this section. A draft of a paper describing the experimental technique and apparatus in more detail is contained in Appendix B. The Seebeck coefficient is determined by applying a temperature gradient along the length of a rectangular bar or right-angle cylinder and measuring the potential differences (ΔV) and temperature gradients (ΔT). The same samples used to measure the electrical conductivity can be used to measure the Seebeck coefficient. The sample is positioned in the center of four parallel Al_2O_3 tubes, each with a Pt-versus-Pt-10% Rh thermocouple emerging from the side of the tube, Figure 5.2. The position of the thermocouple varies for each tube so that a thermocouple contacts the sample at different distances along its length. Four additional solid alumina rods with a Pt wire wrap are used to maintain a parallel positioning of the sample. The Al_2O_3 rods are restrained at the bottom and a slip ring is inserted over the top of the rods to force the thermocouple beads against sample. An auxiliary, non-inductive, externally-controlled cylindrical heater is inserted over the Al_2O_3 rods at one end of the sample to provide a controlled temperature gradient from 10 to 150 degrees K. The unit is then inserted vertically in Al_2O_3 muffle tube with controlled atmosphere and heated inside a resistance-wound furnace. The multi-probe arrangement allows the determination of six ΔT and ΔV about the average temperature (T_a) values. The Seebeck coefficient for T_a is determined from the slope of ΔV versus ΔT.

The experimental measurement with the sample in a vertical test geometry minimizes the potential determinate errors resulting from

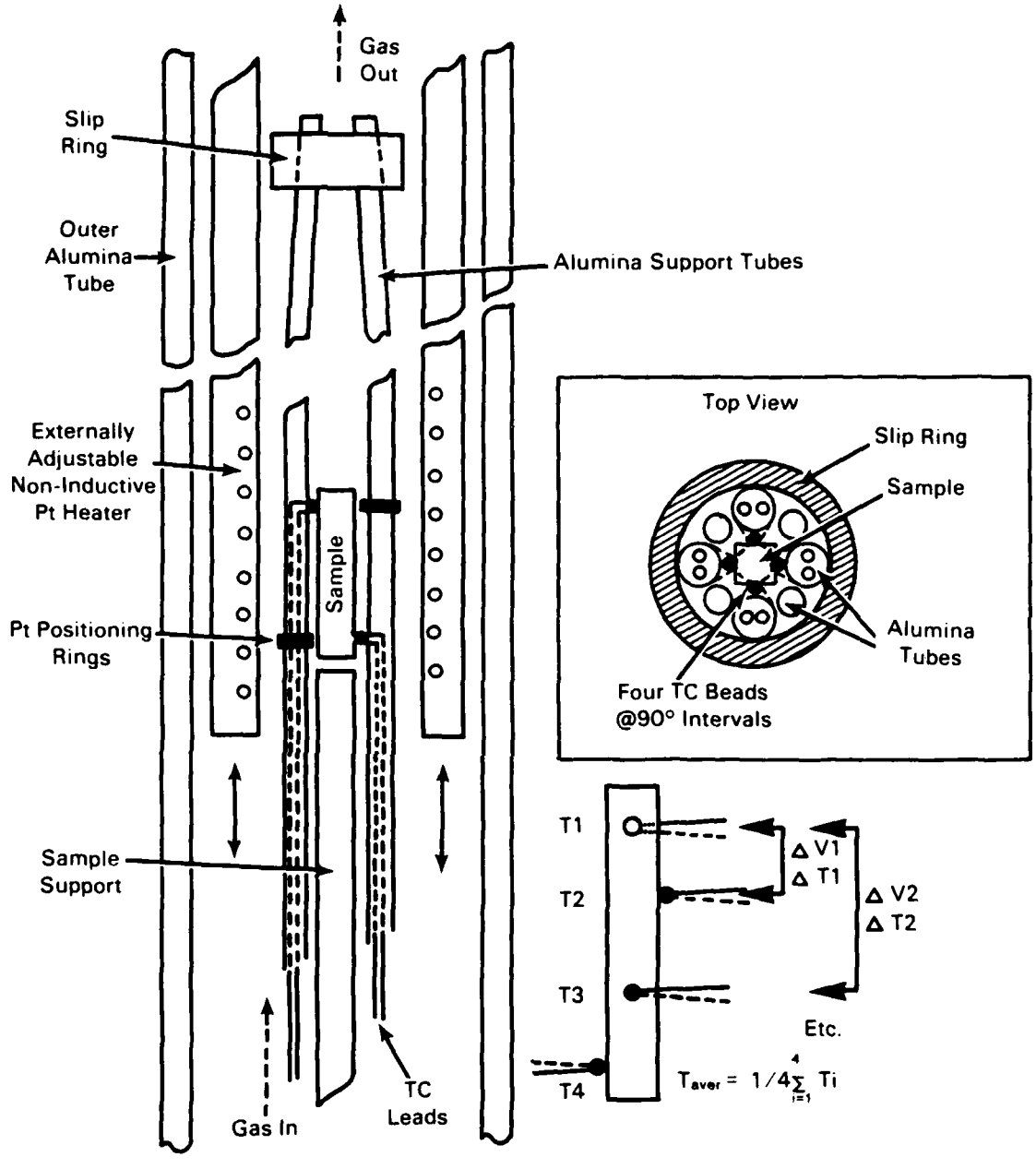

FIGURE 5.2. Interior Details of Thermoelectric Power Apparatus

non-isothermal radial heating in the sample thickness. Radial temperature gradients introduce bias voltage errors that complicate the theoretical interpretation of data, especially when more than one type of charge carrier is present. In addition, the temperature gradient can be controlled to provide the best accuracy optimized for T_a and S. The contact pressure of the thermocouple beads on holding the sample do not require drilling of the sample or the need for contact bonding.

The data acquisition system is computer controlled (Appendix B). The leads from the thermocouples and Pt leads, which function as voltage leads, are hard-wired to a computer-addressable scanner switch-box. Under computer control, the eight potentials are switched to a digital voltmeter, then to the host computer for analysis and storage of the six ΔV and ΔT values about T_a, and the four temperatures. This process requires approximately five seconds and allows repeated checks of raw data. Corrections to the raw data are made for thermocouple calibrations and emf effects from Pt lead wires (referencing to National Bureau of Standards), from which the absolute Seebeck coefficient T_a and determinate errors are calculated.

Because of the rapid acquisition of data, measurements can be made either at thermal equilibrium or during controlled changes in temperature, i.e., <2 K/minute. This allows automation of measurements for any one sample as a function of temperature, e.g., overnight. The data are quickly processed by the operator at the end of the run. The acquisition, evolution and storage of data, the calculation of S and errors, and the plotting and printing are computer controlled, using a special program developed for this purpose. The control of the furnace and auxiliary heater are presently separately controlled but can also be computer controlled, if needed.

The absolute Seebeck coefficient is determined from the least squares analysis of the six ΔV-ΔT data points. This computed value is preferred over using either the origin as a datum point or force-fitting the data through the origin, since these values may bias results. This is

especially true if more than one charge carrier is active and/or if heterogenous distribution of immobile ionic species are present.

The data output for each T_a is compiled and printed. Included are the absolute temperature variation versus distance across the test specimen (upper right), the plot of corrected ΔV versus ΔT, the absolute Seebeck coefficient, the calculations using the origin as data points, and the associated errors.

The sources of error in the measurement of the Seebeck coefficient have been assessed on the basis of indeterminate and determinant errors. Indeterminate errors occur from system variation from assumed boundary conditions and other sources that are often difficult to recognize and eliminate. Of the postulated indeterminate errors (Appendix B), the largest potential source of error occurs from uncertainties in the thermoelectric emf of the Pt lead wires; this translates into an uncertainty of <5% in the absolute value of the Seebeck coefficient when S is <100 $\Delta V/K$. Determinate errors are associated with the measurement of quantities used in calculating the Seebeck coefficient. These errors result from inaccuracies associated with the measurement instruments used (temperature sensors, voltage leads, multiplex scanner contacts, microvoltmeter, etc.) The total 3 σ error in Seebeck coefficient is estimated to be ±2.8%, which translates to a ΔV versus ΔT origin intercept error ($\Delta T_{\Delta V \to 0}/\Delta T_{Max}$) of <2%.

The determinate uncertainties, along with time variations in T_a are used by the controlling computer program to determine when isothermal conditions within the test apparatus have been achieved. When the rate of change in T_a is less than 2 K/minute; origin and 3σ uncertainties are within error analysis limits; and, reproducible emf measurements are observed, the new data will be acquired by the computer and stored for later analysis.

5.4 TRANSFERENCE NUMBERS

In characterizing the high-temperature transport properties of oxide ceramics, it is necessary to separate the electronic and ionic contributions to the total electrical conduction and to determine the dependence on oxygen pressure. It is anticipated that most of the highly-conducting materials considered as high-temperature thermoelectrics are primarily electronically conducting. However, to fully understand the transport properties and to develop models for thermoelectric materials, selective studies of transference numbers are required. In addition, a more accurate measurement at high electronic-transference number values is required than what is now considered standard technique. Of the three experimental techniques--electrochemical cell, polarization and coulometric titration cell--the latter offers the measurement sensitivity ($0.000 < t_i < 0.9999$) necessary to the study of high electronically conducting thermoelectric materials.

The solid-state coulombic cell, Figure 5.3, is used to control the composition of nonstoichiometric phases, providing the direct measurement of transference numbers and the determination of the mobility of charge carriers. In addition, this technique minimizes the problems of polarization and of the difficulty of measurements with transference number values >0.99 and <0.1.

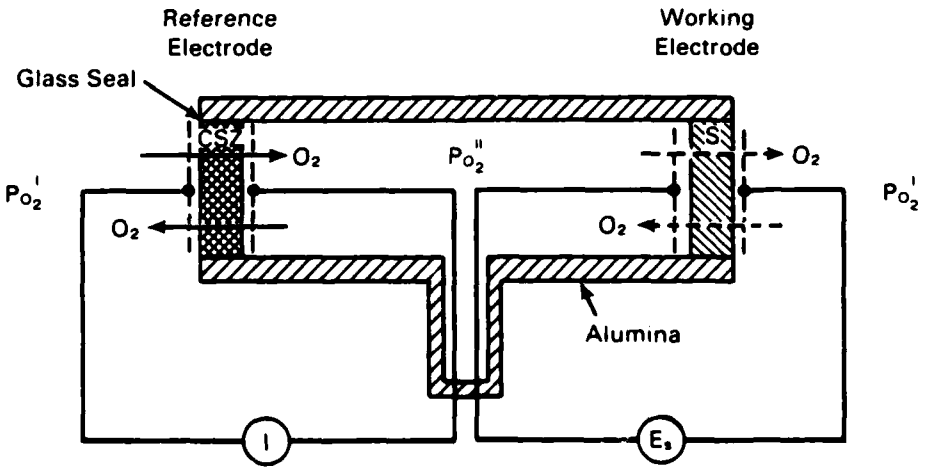

FIGURE 5.3. Coulometric Titration Cell

The coulombic titration cell uses separate reference and working electrodes enclosed in an Al_2O_3 tube to measure oxygen permeability. Oxygen is pumped in and out of the interior of the cell by application of a known emf to the reference CaO-stabilized ZrO_2 electrode. The oxygen potentials across the working electrode are established at equilibrium and the measured change in emf, E_s, is used to determine the transference number. The mobility of the minority electronic carrier is determined by the rate of change in E_s following a step change in Po_2. This technique is being partially developed under a Department of Energy program. Several HfO_2-PrO_2-In_2O_3 compositions are being evaluated at Marquette University using this technique for applicability to this program and to provide measurement references.

5.5 LASER RAMAN SPECTROSCOPY

Laser Raman Spectroscopy is used to provide information on the molecular structure, stoichiometry and solid-state phase transformations. These data are especially valuable in determining changes due to compositional variations and doping or atmospheric variations that relate to the transport properties of high-temperature thermoelectric materials. Further discussion is included in Section 6.0.

5.6 CALCULATION OF THE FIGURE OF MERIT

The figure of merit was calculated by:

$$ZT = \frac{S^2\sigma}{\lambda} * T$$

The experimental data for the Seebeck coefficient (S, μ V/K), electrical conductivity (σ, ohm-cm)$^{-1}$, and thermal conductivity (λ, W/m-K) were fitted to equations of the form:

$$S = A + BT + CT^2 + DT^3$$

$$\log \sigma = A + \frac{B}{T}$$

$$\lambda = \frac{1}{A + BT} \quad \text{or} \quad A + BT + CT^2 + DT^3$$

Using a computer program, these equations were used to calculate ZT as a function of temperature. The calculated values for ZT, σ, λ, S and the coefficients (A, B, C, and D) used to make the calculations are given in Appendix A.

6.0 EXPERIMENTAL RESULTS FOR OXIDE MATERIALS

The experimental results for different compositions of $YCaCrO_3$, $YMgCrO_3$, $YSrCrO_3$, $LaSrMnO_3$, and $HfO_2(ZrO_2)$-R_xO_y-In_2O_3 are discussed below. In some cases, the relationship of transport property data to the theories developed in section 4.0 is also discussed.

6.1 $(In_2O_3)_x \cdot (SnO_2)_{1-x}$

Mixed oxides based on In_2O_3 and SnO_2 were briefly examined as possible thermoelectric materials because of their very high electrical conductivity.[a] The materials exhibit properties characteristic of an n-type highly degenerate semiconductor with high electrical conductivity and low thermal conductivity. The electrical conductivity generally increases as the indium content increases with the greatest increase between 7 and 30 mole%, Figure 6.1.[6.1] At higher In_2O_3 concentrations, compositions of the electrical conductivity increase is much smaller. A maximum conductivity is observed near 95 mole% In_2O_3 and is about 10 times greater than for pure In_2O_3. The Seebeck coefficient is negative and becomes more negative with temperature in nearly a linear manner, Figure 6.2. The S values are typical of a degenerate semiconductor or a metal.

Thus, we may interpret S as being a result of transport of electrons in a degenerate broad band. For such a case,

$$S = -\frac{\pi^2}{3}\left(\frac{k}{e}\right)\frac{kT}{E_F} = \left(\frac{7.35}{E_F(eV)}\right)\left(\frac{T}{300}\right)\ \mu V/K$$

The conductivity data indicate the E_F lies a few tenths of an eV into the conduction band.

(a) The fabrication, electrical conductivity and crystallographic studies for these oxides were conducted under a U.S. Department of Energy program at Battelle. Because of their significance, these data are discussed here.

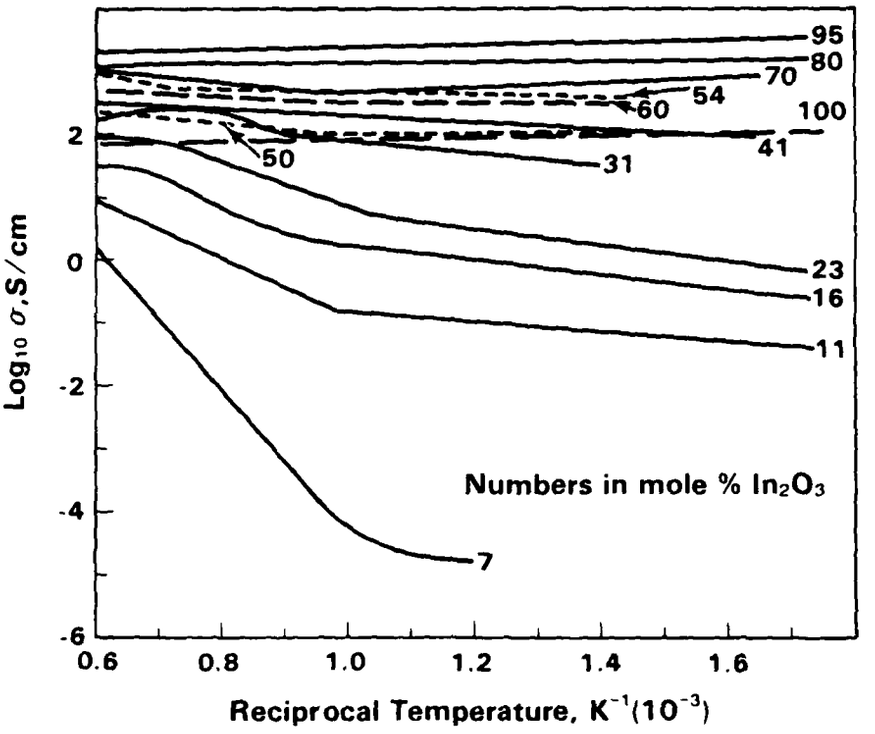

FIGURE 6.1. Electrical Conductivity of $In_2O_3 \cdot SnO_2$. The In_2O_3 content is shown in mole%.

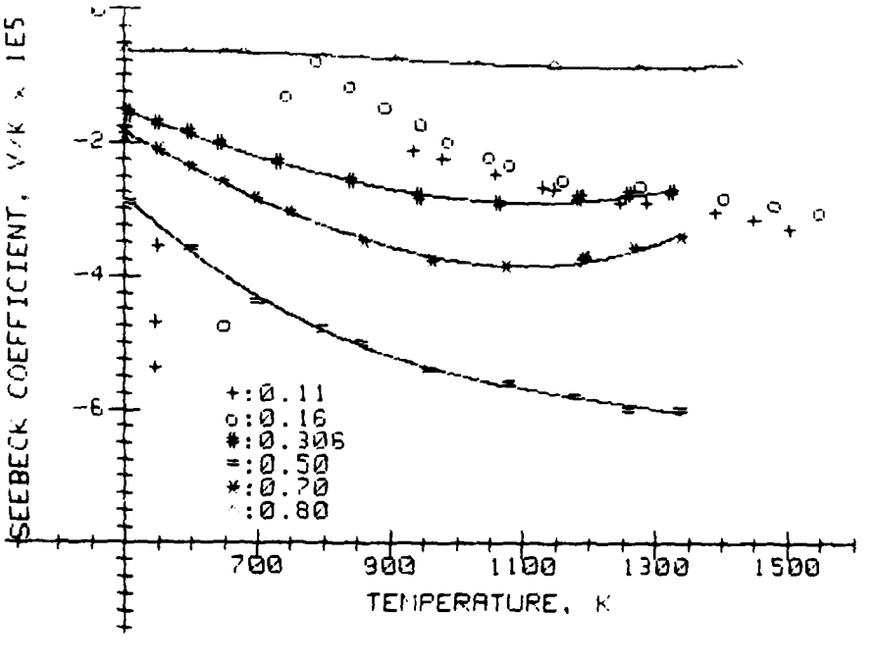

FIGURE 6.2. Seebeck Coefficient for $(In_2O_3)_x \cdot (SnO_2)_{1-x}$

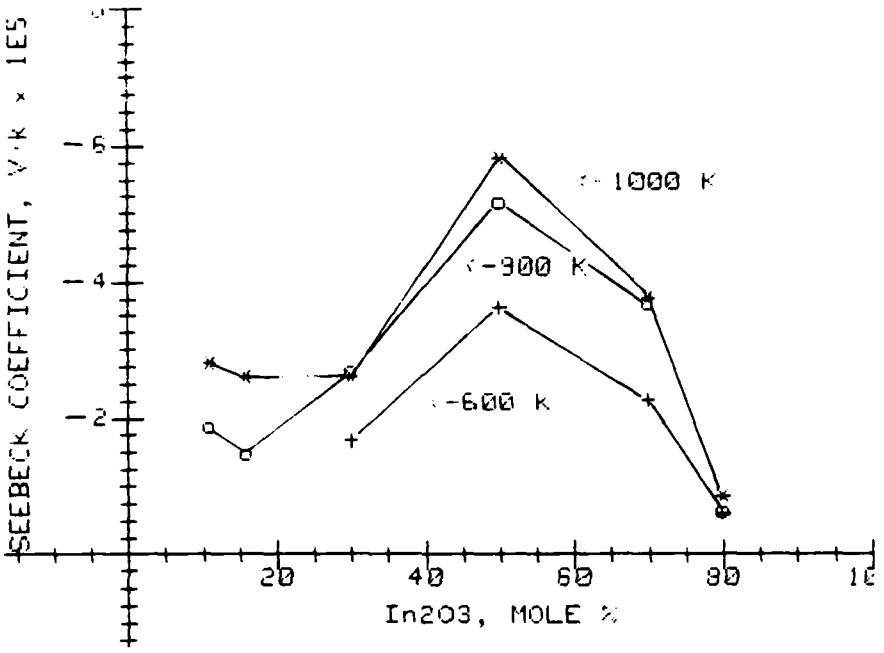

FIGURE 6.3. Seebeck Coefficient Versus In_2O_3 Content

The Seebeck coefficient is plotted versus mole% In_2O_3 for mixed compositions In_2O_3 and SnO_2 for various temperatures, Figure 6.3. The data suggest that a phase change occurs near 50% In_2O_3 and at about 30% In_2O_3. The dependence of S with mole% In_2O_3 data for compositions between these phases can be interpreted by considering S to be a result of two phases acting in parallel. In such a case, the measured value of S is given by

$$S = \frac{S_1\sigma_1 + S_2\sigma_2}{\sigma_1 + \sigma_2}$$

where 1 and 2 refer to the two phases. In addition, the variations in σ with In_2O_3 content also suggest that new phases are forming between 30 and 50 mole%.

The thermal conductivity for four measured samples containing 11, 16, 70, and 80 mole% In_2O_3 is low, Figure 6.4, <1 W/m-K. There does not appear to be a consistent variation in thermal conductivity relative to In_2O_3 for the four compositions. It can be supposed that microstructural variations

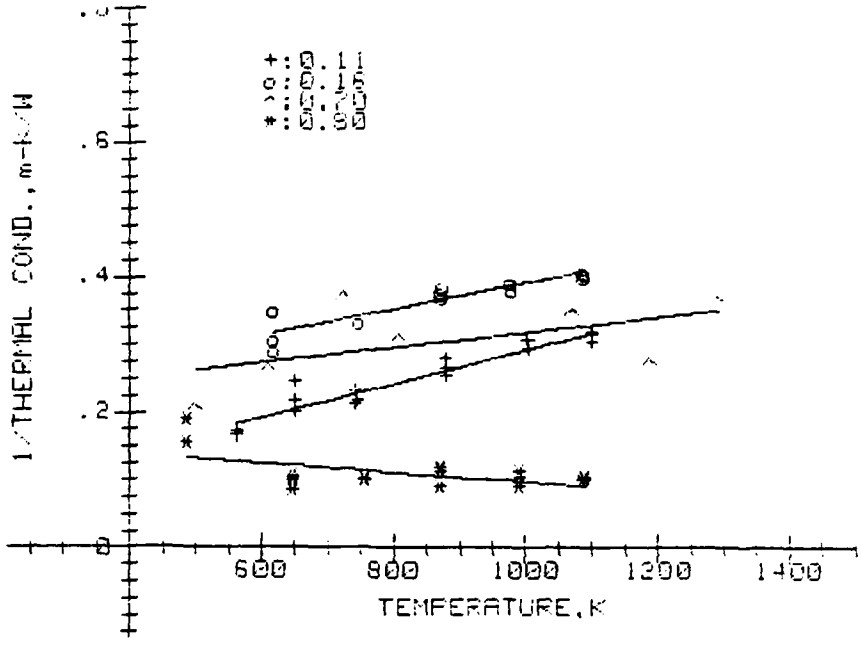

FIGURE 6.4. Thermal Resistivity for $(In_2O_3)_x \cdot (SnO_2)_{1-x}$

may be more responsible for the variation than the electrical transport properties or composition. Further study is required to resolve these variations.

The formation of a crystalline phase between 30 and 50 mole% In_2O_3 is also indicated from x-ray diffraction and laser Raman spectroscopy. A rhombohedral phase was found with x-ray diffraction between 30 and 42 mole% with 95% rhombohedral phase at 38.3 mole% In_2O_3. Laser Raman spectroscopy of sample surfaces after Seebeck coefficient measurements (Figure 6.5) shows free SnO_2 and/or In_2O_3 except for the 50-50% composition, where a solid solution is clearly indicated, e.g., only two spectral features at 489 and 678 wave numbers). Raman spectroscopy also indicates a compound between 30 and 38 mole% In_2O_3. These results appear consistent with the electrical conductivity and Seebeck coefficient measurements, specifically the maximum in S near 50 mole% In_2O_3, the relatively constant S between 30 and 40 mole% In_2O_3, and the high σ above approximately 30 mole% In_2O_3, and the sharp decrease in σ below 30 mole% In_2O_3.

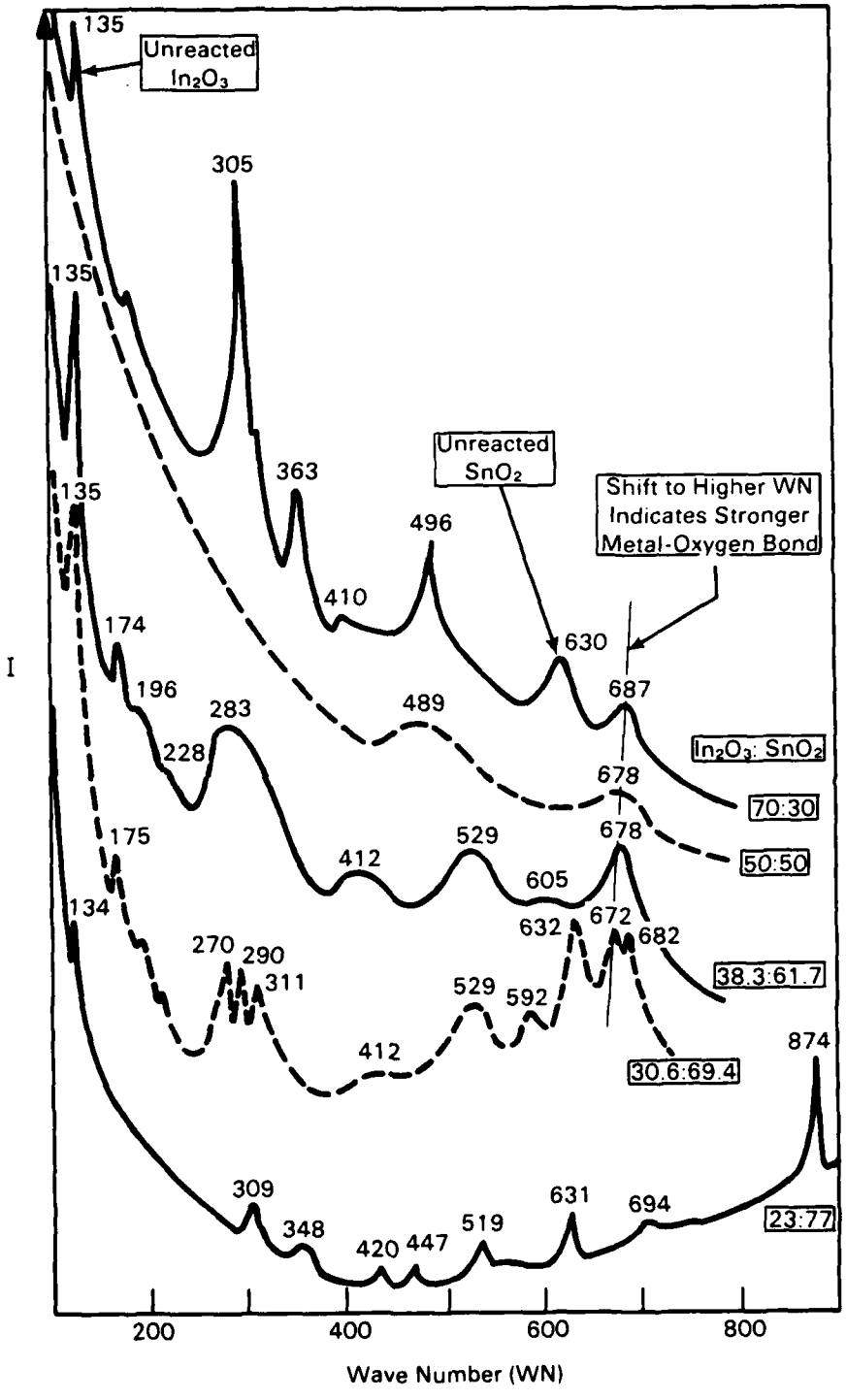

FIGURE 6.5. Laser Raman Spectra for $In_2O_3 \cdot SnO_2$ Compounds

The figures of merit for four In_2O_3-SnO_4 are shown in Figure 6.6. For the 11, 16, and 80 mole% In_2O_3, the values are very low, <0.01. However, for the 70 mole%, ZT is small at low temperatures and approaches 0.1 at 1200 K. Although λ was not measured for 50 mole% in_2O_3, assuming a value near 3 W/m-K, the figure of merit is about 50% higher than that for the 70 mole% In_2O_3. However, ZT values are low as expected for this broad-band, degenerate semiconductor. For these materials to be of practical interest, the Seebeck coefficient must be significantly larger.

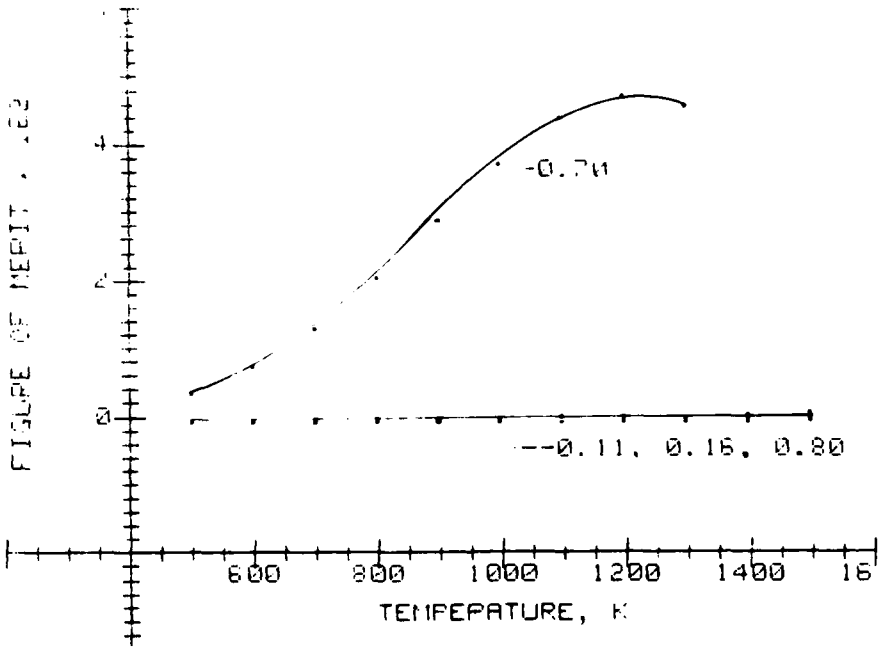

FIGURE 6.6. Figure of Merit for $(In_2O_3)_x \cdot (SnO_2)_{1-x}$

6.2 CHROMITES

A large number of oxides crystallize in the cubic ABO_3 perovskite structure or slight distortions thereof. Many of these materials exhibit semiconducting behavior when doped with divalent metals. In particular, moderate Seebeck coefficient values and high electrical conductivity have been reported for some of these materials.[6.2] Since there can be several components in a given compound, it is possible that the lattice component of the thermal conductivity can be reduced to a relatively low value. Thus, these materials appear to have good potential as a thermoelectric material. In addition, these compounds appear to be nondegenerate and are narrow-band semiconductors. Thus, the perovskites were chosen as a class of materials for detailed investigation.

Preliminary results have been obtained for $Y_{1-x}Ca_xCrO_3$, $Y_{1-x}Sr_xCrO_3$, and $YMg_xCr_{1-x}O_3$ compounds. The first class of materials have a divalent impurity substituted on the A site, while the second class have a divalent impurity substituted on the B site. Preliminary experimental results for the electrical transport properties of these materials are reported and the results are discussed in terms of the theory developed in Section 3.0.

6.2.1 $Y_{1-x}Ca_xCrO_3$

Electrical and thermal conductivity, Seebeck coefficient, and calculated figure of merit have been determined for three levels of calcium concentration, Figures 6.7 through 6.10. The electrical conductivity and Seebeck coefficient both increase with temperature. The electrical conductivity for x = 0.02 and x = 0.1 can be written as

$$\sigma = \sigma_o \, T^{-1} \exp\left(\frac{E_A}{kT}\right)$$

The electrical conductivity data for x = 0.2 suggest that two conduction mechanisms are involved, as indicated by the two liner variations of Log σ

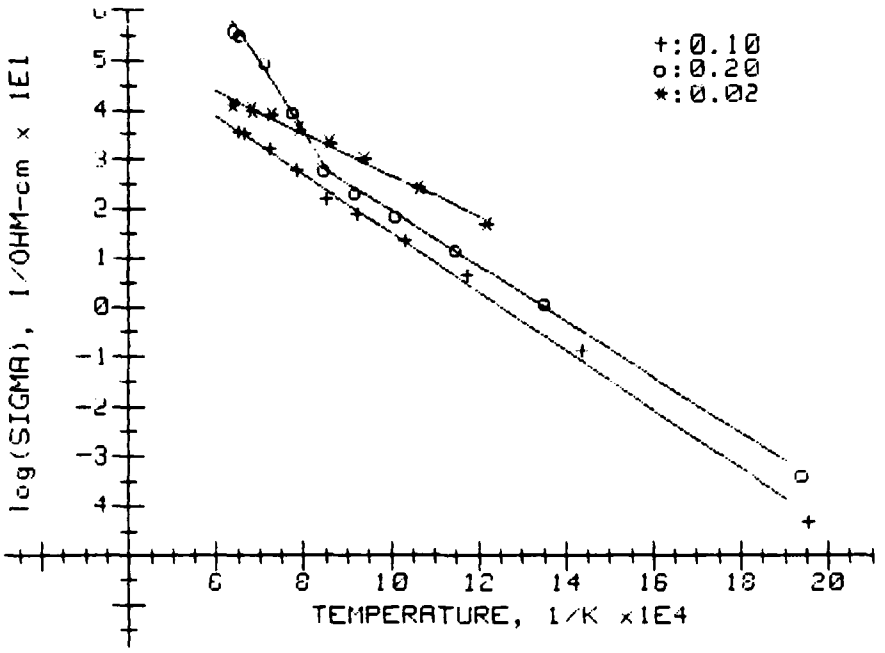

FIGURE 6.7. Electrical Conductivity for $Y_{1-x}Ca_xCrO_3$

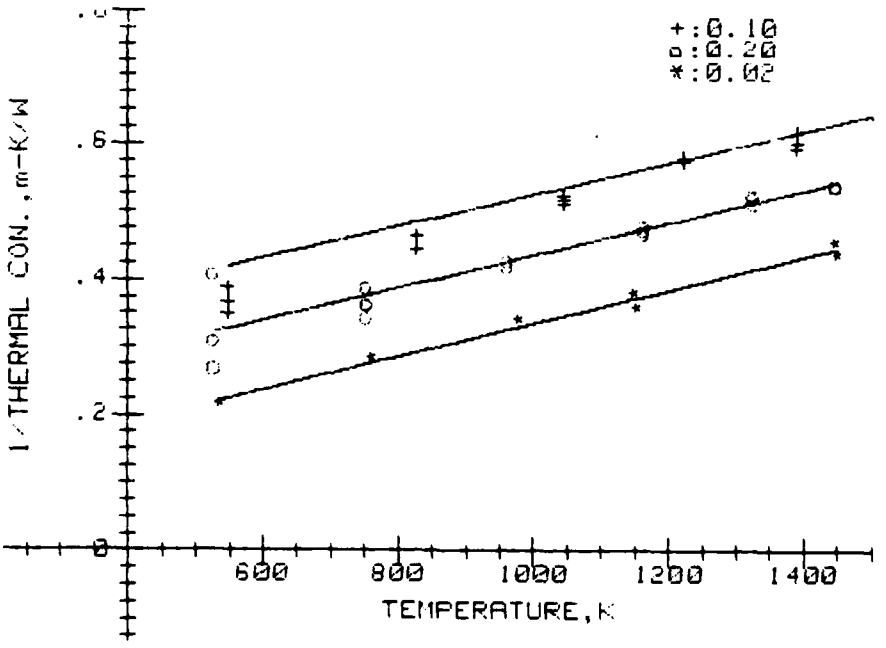

FIGURE 6.8. Thermal Resistivity for $Y_{1-x}Ca_xCrO_3$

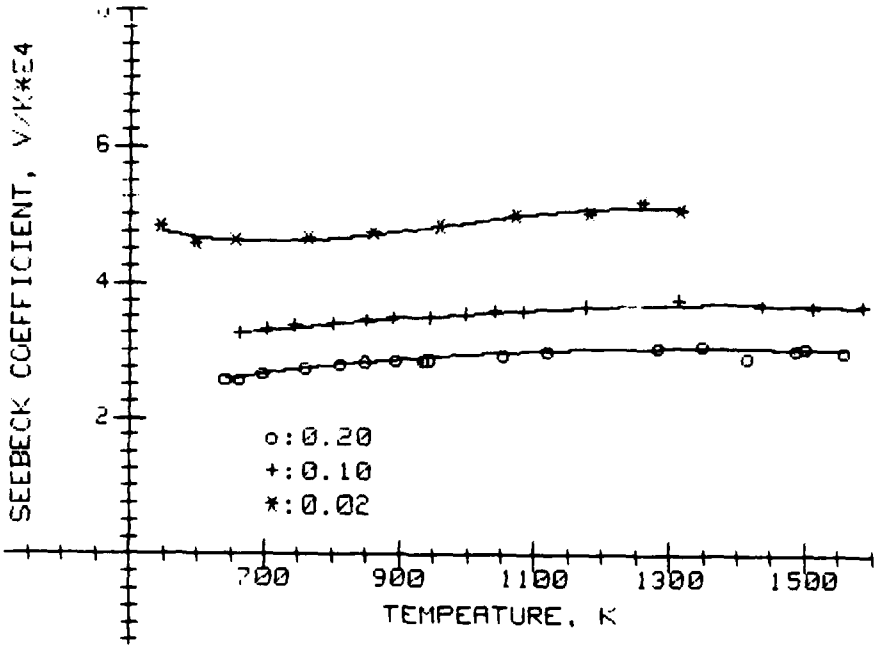

FIGURE 6.9. Seebeck Coefficient for $Y_{1-x}Ca_xCrO_3$

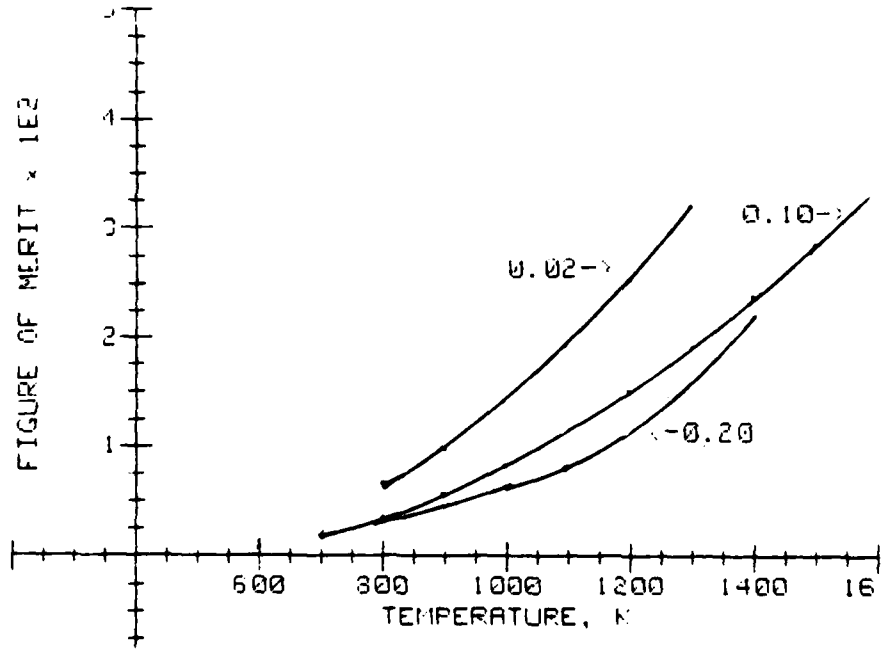

FIGURE 6.10. Figure of Merit for $Y_{1-x}Ca_xCrO_3$

versus K^{1} at high and low temperatures. However, it appears that the same activation energy that fits the x = 0.02 and x = 0.1 data is appropriate at lower temperatures for x = 0.2. The Seebeck coefficient for x = 0.02, x = 0.1, x = 0.2, can be expressed as

$$S = A + BT$$

up to 1200 K.

These results strongly suggest that electrical transport in this class of perovskites is due to small polaron conduction. The value of B is not very sensitive to the composition. As discussed in Section 4.2, B is proportional to J^2, where J is the overlap integral between hopping sites. Apparently, J is not changing significantly with x, or there are compensating effects.

The parameter A is dependent upon the location of Fermi level, E_F. A possible band structure for $Y_{1-x}Ca_xCrO_3$ is shown in Figure 6.11. As x is increased, the hole concentration in the π-band increases due to formation of Cr^{4+} sites. As a result, E_F moves closer to the π-band edge, which decreases A.

Future work will involve further theoretical and experimental studies of these materials. Eventually, formation of a model for this system and similar materials, such as the $La_{1-x}Sr_xCrO_3$ will lead to an approach that yields materials with larger σS^2 values. It will be particularly important to understand changes in transport properties which result from substitution of divalent ions on either A or B sites.

6.2.2 $Y Mg_x Cr_{1-x} O_3$

The electrical properties for this class of perovskites can also be interpreted in terms of small polaron transport. For these Mg-doped chromites, it is reported that Mg is introduced on only the B-sites,[6.3] whereas Ca was introduced on the A sites for $Y_{1-x}Ca_xCrO_3$. The electrical

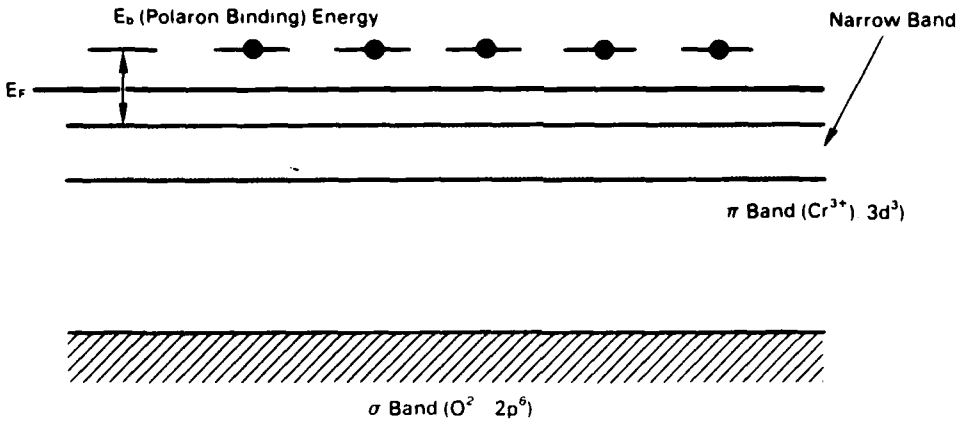

FIGURE 6.11. Proposed Band Model

conductivity, thermal conductivity, and Seebeck coefficient (Figures 6.12 through 6.14) decreased with increasing Mg. The figure of merit was not greatly affected by varying the value of x (Figure 6.15). The parameter A also appears to increase as x increases from 0.02 to 0.05. Further investigation of these Mg-containing yttrium chromites is required before an adequate model can be developed to account for the transport property differences due to variations in composition and substitution on the A or B sites.

6.2.3 $Y_{1-x}Sr_xCrO_3$

The transport properties for $Y_{1-x}Sr_xCrO_3$ materials exhibit different behavior. The electrical and thermal conductivity and Seebeck coefficient for x = 0.2 vary with temperature in a similar manner as the other A site substituted chromites, Figure 6.16 through 6.18. A possible interpretation of the x = 0.2 data could involve small polaron transport. In the case of x = 0.1, the Seebeck coefficient data could be interpreted as being due to "hole" transport in a broad band. Thus, it appears the type of transport for x = 0.1 is different from x = 0.2. The figures of merit for the two chromite compositions are also significantly different, Figure 6.19.

It is reported that as the metal doping concentration of Ca, Mg, or Sr in $LaCrO_3$ increase, the perovskite structure reverts to a rhombohedral structure.[6.3] This structure change occurs near x = 0.1 for $La_{1-x}Sr_xCrO_3$.

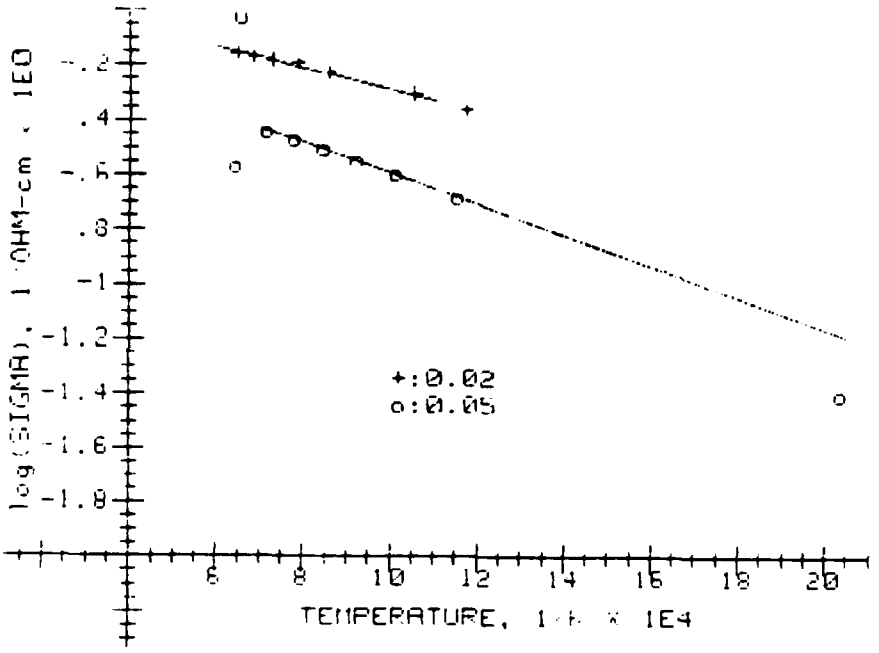

FIGURE 6.12. Electrical Conductivity for $YMg_xCr_{1-x}O_3$

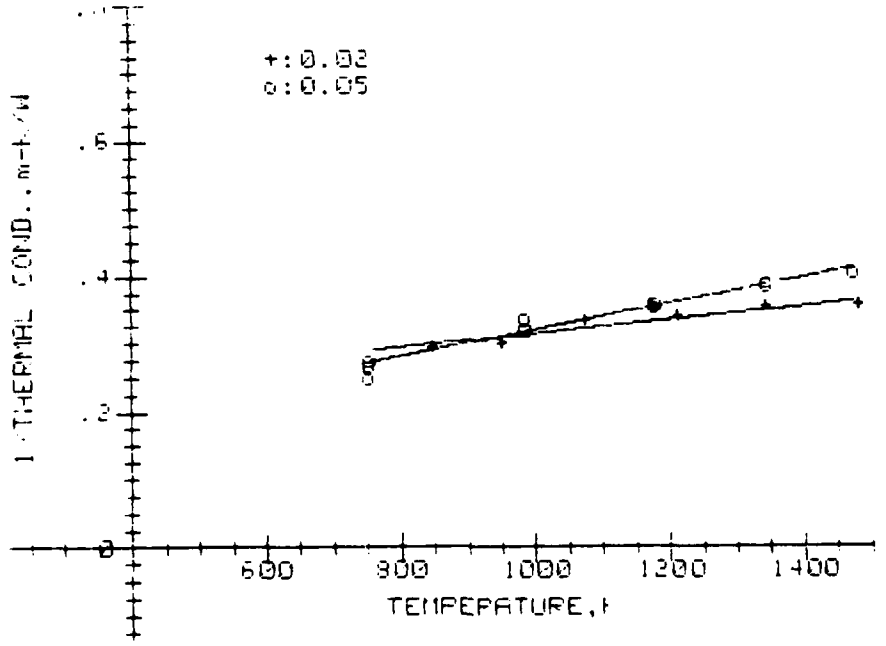

FIGURE 6.13. Thermal Resistivity for $YMg_xCr_{1-x}O_3$

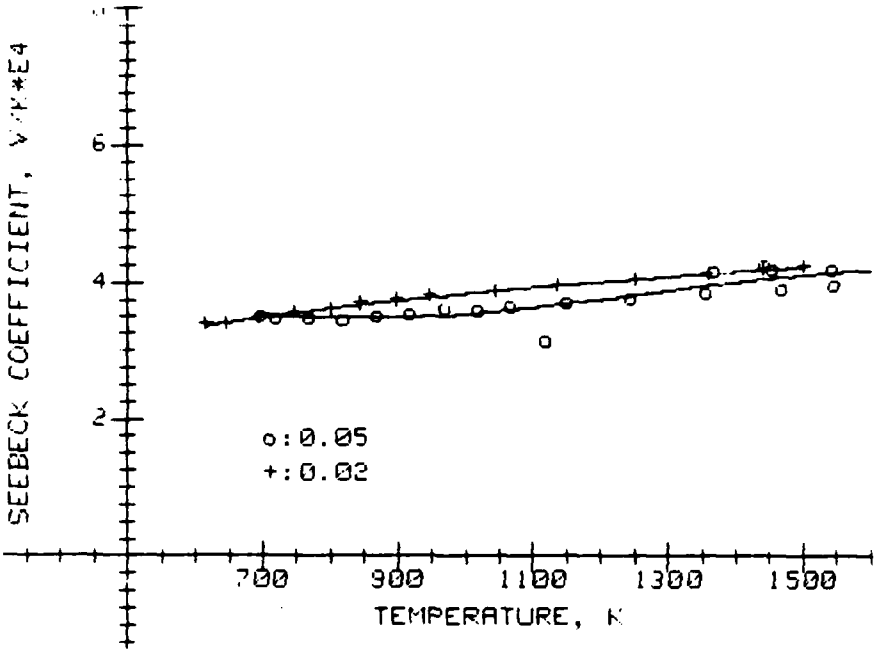

FIGURE 6.14. Seebeck Coefficient for $YMg_xCr_{1-x}O_3$

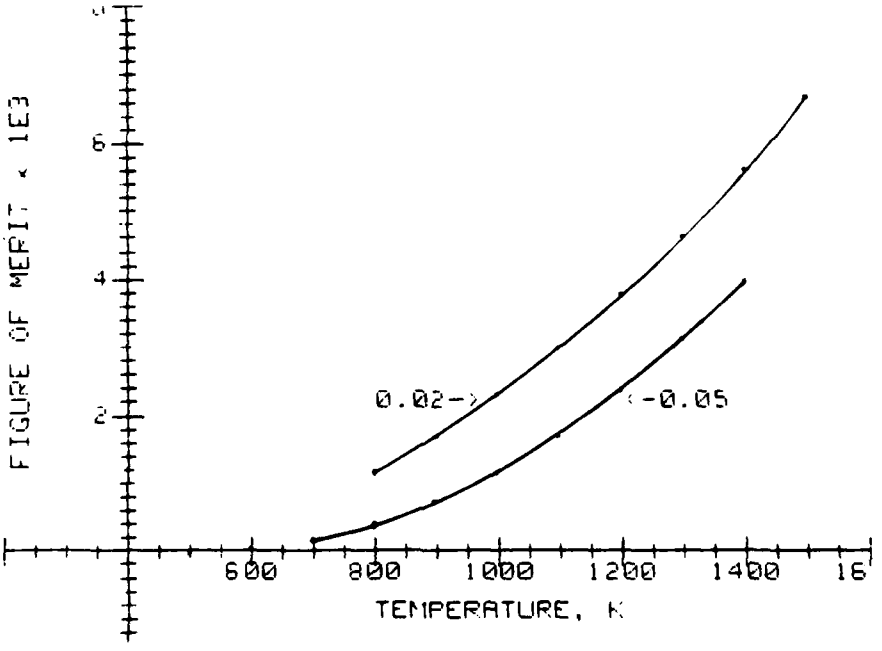

FIGURE 6.15. Figure of Merit for $YMg_xCr_{1-x}O_3$

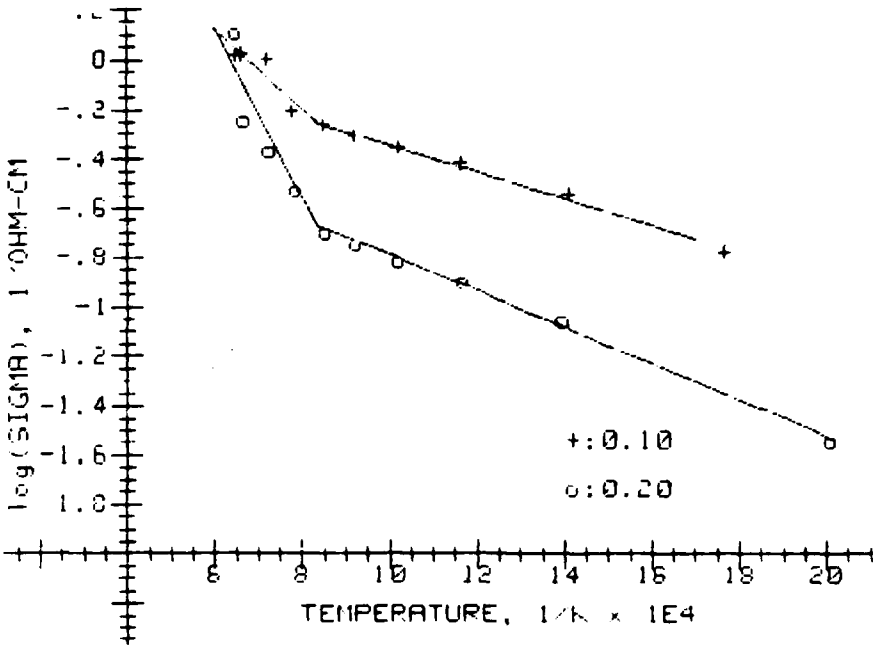

FIGURE 6.16. Electrical Conductivity for $Y_{1-x}Sr_xCrO$

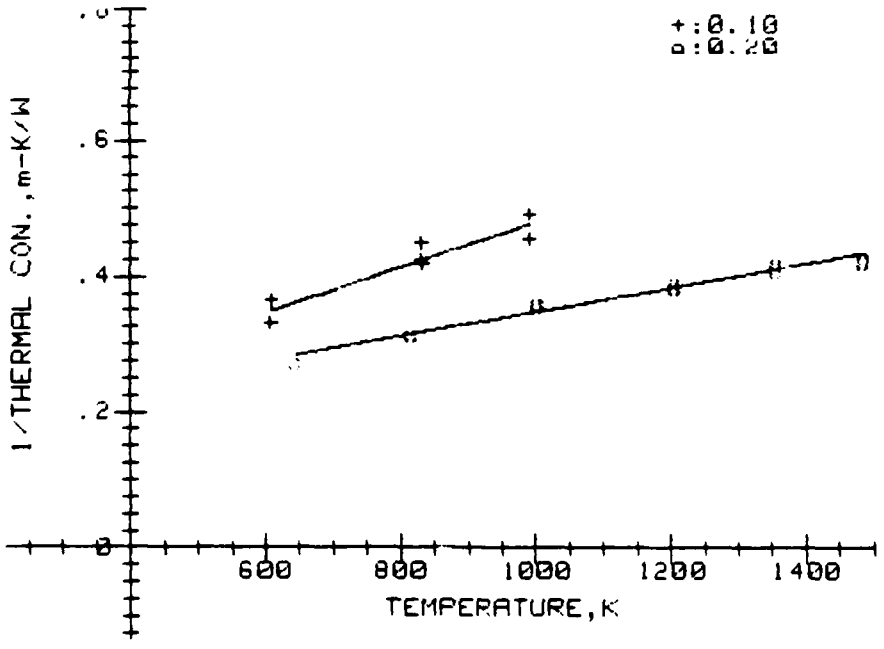

FIGURE 6.17. Thermal Resistivity for $Y_{1-x}Sr_xCrO$

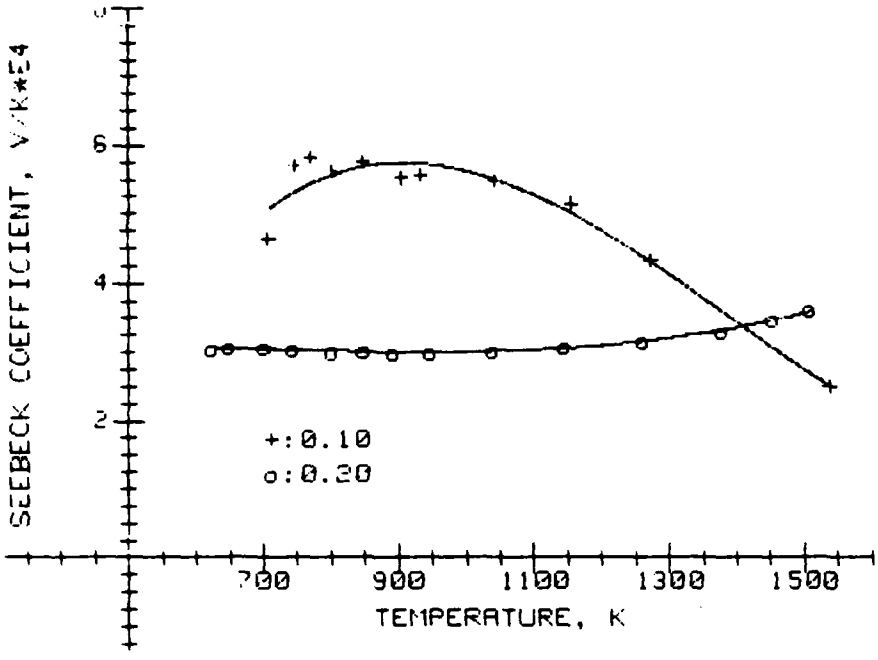

FIGURE 6.18. Seebeck Coefficient for $Y_{1-x}Sr_xCrO_3$

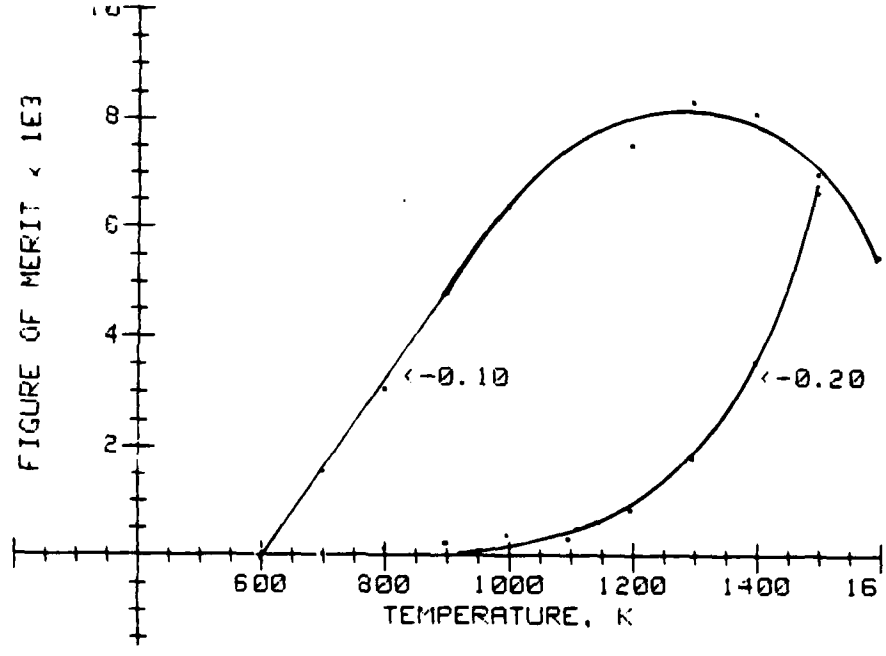

FIGURE 6.19. Thermal Resistivity for $Y_{1-x}Sr_xCrO_3$

This change in crystallographic structure could significantly influence the defect structure and electronic transport and account for some of the results observed in this study. Similar changes can be expected for the isomorphic $YCrO_3$ compositions.

The Raman spectra for the two $Y_{1-x}Ca_xCrO_3$ compositions after heat treatment to 1775 K in air show distinct differences as well as similarities. The Raman spectra results suggest that $Y_{0.8}Sr_{0.2}CrO_3$ exhibits weaker oxygen-to-metal bonding and possible differences in crystal structure (i.e., formation of the rhombohedral structure). The significant differences in electrical conductivity, thermal conductivity, and Seebeck coefficient suggest that the crystalline structure and/or metal-oxygen bonding of the unit cell has important effects on all transport properties.

6.2.4 Chromites General

The yttrium chromite results for all compositions are summarized in Table 6.1. The initial theoretical modeling of test results indicates that the transport mechanism for the chromites is by small polaron transport, regardless of the substitutional divalent foreign cation on the A or B site (i.e., Mg, Ca, Sr). The thermal conductivity does not appear to be highly sensitive to divalent doping on the A or B site, although a trend toward decreasing conductivity from approximately 3 to 2 W/m-K is observed upon increasing the divalent cation size (i.e., ionic radii: Mg = 0.69Å; Ca = 0.99 Å; Sr = 1.13 Å; Ba = 1.35 Å). The increase in thermal conductivity for $Y_{1-x}SrCrO_3$, going from x = 0.1 to x = 0.2, appears associated with a phase change in the material.

Further studies are warranted to understand the effects (if any) of A- versus B-site substitutional doping on small polaron transport and Seebeck coefficient. The effects of lattice stress (relaxation of the unit cell versus elongation of the unit cell) are also an an area that requires further theoretical and experimental investigation. Increasing lattice stress can cause changes in the perovskite structure which has 12 and 6 coordination by oxygen ions for A and B sites, respectively, to 6 and 6 coordination for A and B sites when the suggested rhombohedral structure is formed by increasing dopant concentration.[6.4] The structural induced

TABLE 6.1 Summary of Preliminary Chromite Test Results at 1000 K in Air

System ABO_3	σ 1/ohm-cm	λ W/m-K	S μV/K	ZT (1000 K)	
$Y\ Mg_{0.02}Cr_{0.98}O_3$	0.516	3.17	383	0.0024	
$Y\ Mg_{0.05}Cr_{0.95}O_3$	0.254	2.74	389	0.0014	
$Y_{0.95}Mg_{0.05}CrO_3$	0.254	3.11	389	0.0012	
$Y_{0.98}Ca_{0.02}CrO_3$	1.83	2.98	489	0.0146	
$Y_{0.9}Ca_{0.1}CrO_3$	1.41	2.08	322	0.0073	Run 1
	1.41	2.00	355	0.0089	Run 2
$Y_{0.8}Ca_{0.2}CrO_3$	1.57	2.33	295	0.0058	
$Y_{0.9}Ca_{0.1}CrO_3$	0.458	2.23	563	0.0065	
$Y_{0.8}Sr_{0.2}CrO_3$	0.164	2.91	301	0.00051	

change may be responsible for the observed decrease in ZT with increasing x in $Y_{1-x}M_xCrO_3$ with M = Mg, Ca, and Sr (Table 6.1). Theoretical modeling of electrical and thermal transport properties needs to consider associated effects of structural variance.

6.3 $HfO_2(ZrO_2)$-R_xO_y-In_2O_3

The HfO_2-R_xO_y-In_2O_3 compound represents another class of highly conducting oxides for high-temperature thermoelectric materials. Previous studies have shown these oxides and the isomorphic ZrO_2 compositions exhibit high electronic conductivity and low thermal conductivity with high-temperature stability. In addition, they represent a different class of oxides with pyrochlore and rhombohedral structures than indium-tin oxides or chromites. However, the thermoelectric properties have not been studied. Previous work has been conducted on these oxides under DOE programs for advanced energy conversion for fuel cells and MHD, and these background transport and phase equilibrium data are used as a base for studying the thermoelectric
application.

Two compositions that had previously exhibited high electrical conduction[6.5] were selected for study, 0.30 In_2O_3·0.033 Yb_2O_3 0.20 PrO_2·0.467 HfO_2 (LLL) and 0.433 In_2O_3·0.036 Y_2O_3·0.035 Tb_4O_7·0.496 HfO_2 (MMM).

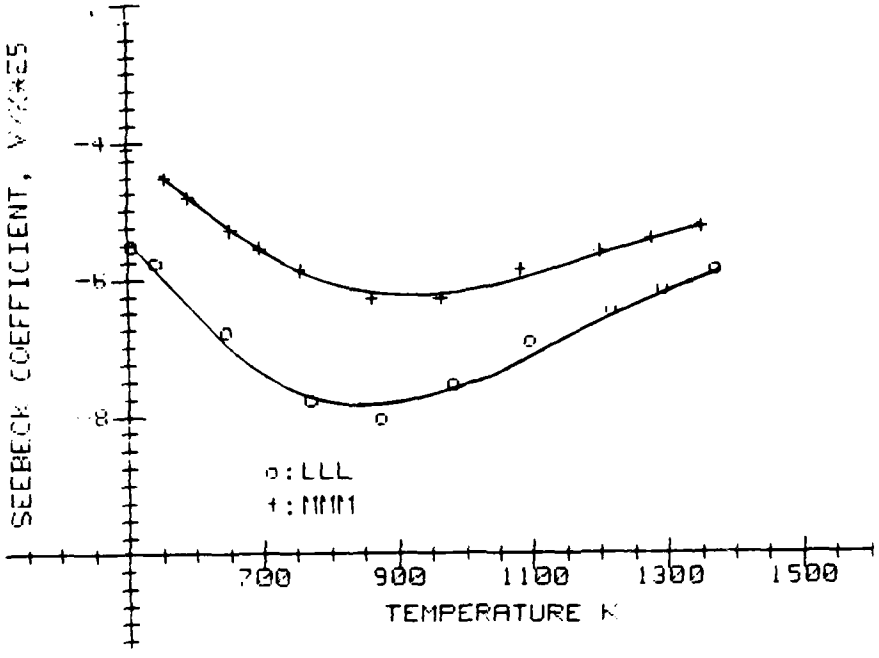

FIGURE 6.20. Seebeck Coefficient for LLL and MMM

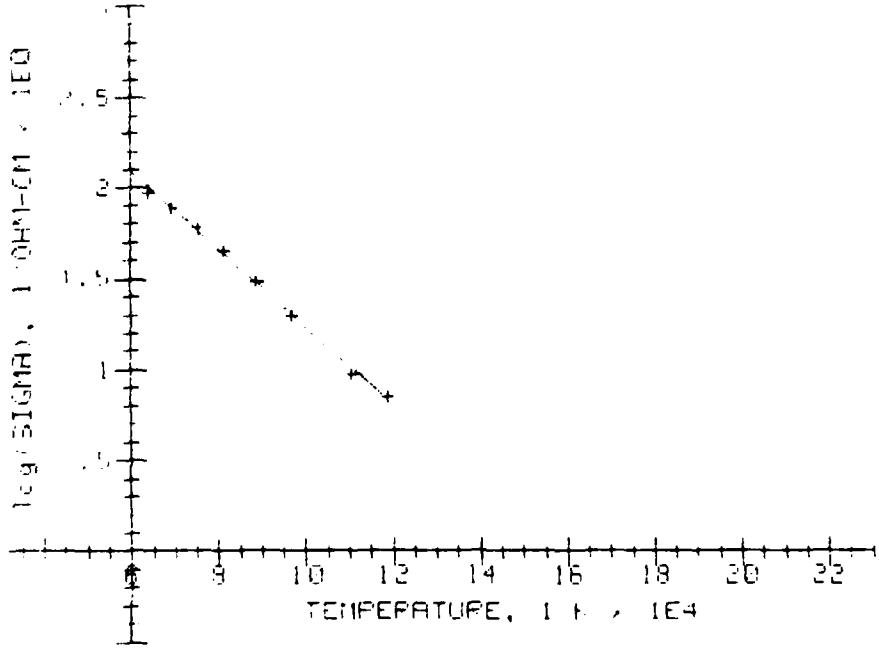

FIGURE 6.21. Electrical Conductivity for MMM

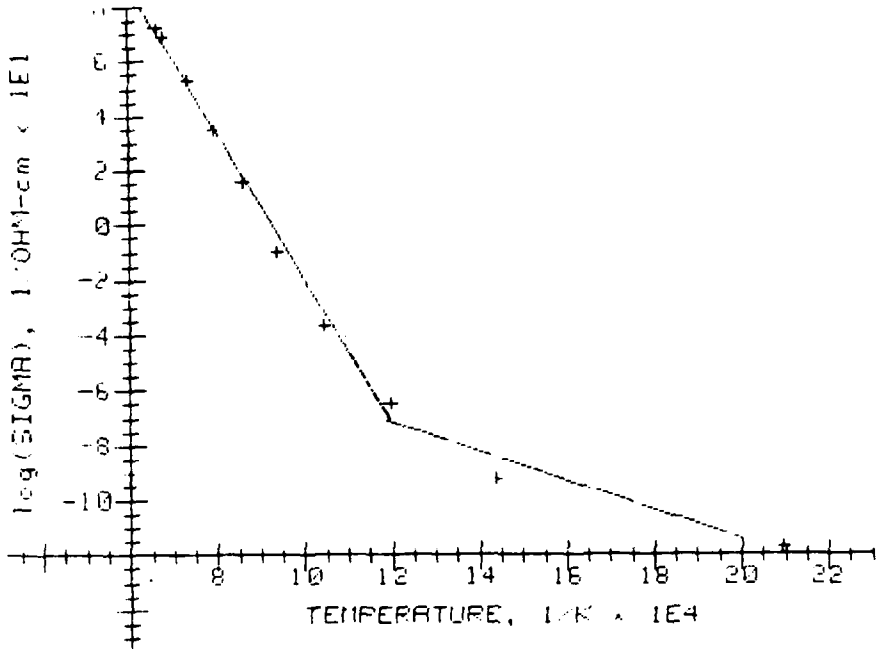

FIGURE 6.22. Electrical Conductivity for LLL

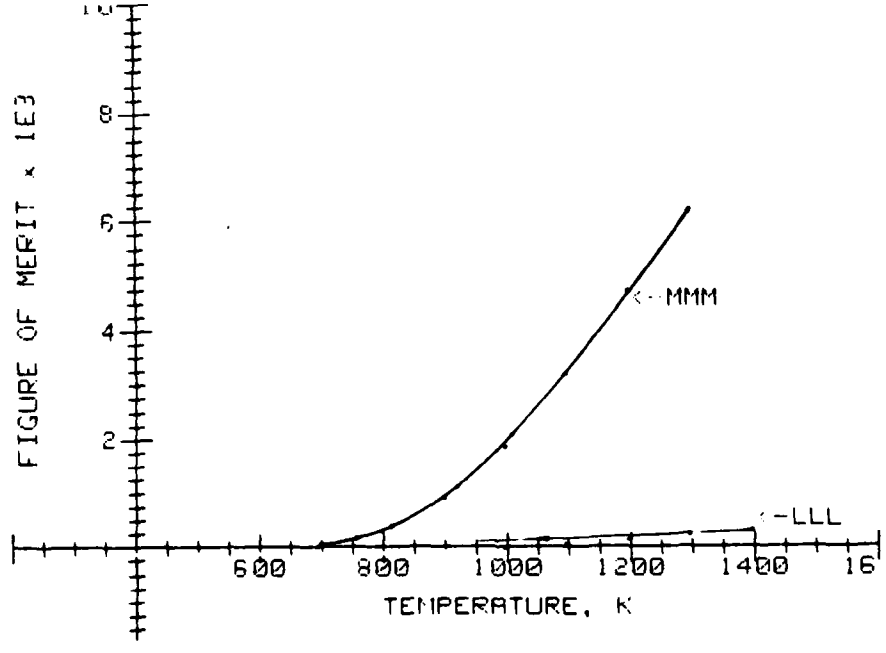

FIGURE 6.23. Figure of Merit for LLL and MMM

Because of the differences in composition and structure, differences in σ, λ, and S were expected and observed, Figures 6.20 through 6.22. The MMM composition exhibits higher electrical conductivities and lower Seebeck coefficients with resultant higher figure of merit, Figure 6.23. However, the moderate σ values and S values <100 μV/K result in ZT values of less than 0.01 for both LLL and MMM, even at high temperatures.

The Seebeck coefficients are negative with values below 100 μV/K. Both exhibit a maximum value near 900 K, Figure 6.20, which corresponds to the temperature for the change in slope of the log σ versus K^{-1} curve for the LLL sample, Figure 6.22. The LLL is a two-phase oxide with pyrochlore and fluorite phases. This two-phase structure may explain the above results and also suggests possible compensating effects for the thermoelectric properties or changes in conducting mechanism.

Other compositions of HfO_2-R_xO_y-In_2O_3, now being studied under the DOE programs, have higher electrical conductivities and are single-phase oxides. In addition, compositions of ZrO_2-R_xO_y-In_2O_3 with single-phase structures are also being prepared for study under the same programs. The thermoelectric characteristics of these materials will be studied when available.

6.4 MANGANATES

A specimen of $La_{0.9}Sr_{0.1}MnO_2$ was investigated to determine the electrical/thermal properties of this perovskite-type structure. Thermal conductivity, electrical conductivity and Seebeck coefficient were measured over a range of temperatures from 473 to 1373 K. A high electrical conductivity (ranging from 56.2 to 13.2 $(ohm\text{-}cm)^{-1}$ that increases with increasing temperature) was offset by a low Seebeck coefficient (ranging from +21.5 to +29.01 μV/K, respectively). The measured thermal conductivity variation of 1.43 to 2.50 W-m K with temperature, however, is consistent with values observed for other oxide systems (i.e., sections 6.1 to 6.3). The Seebeck coefficient was positive, indicating the major electronic carrier in this material was holes. The figure of merit ranged from a maximum of 0.006 at 1373 K to 0.0009 at 473 K.

7.0 FUTURE DIRECTION

Future research will focus on a more in-depth study of narrow-band oxides that conduct predominantly by small polarons. The chromites ($A\ CrO_3$) will initially be emphasized and a composition matrix (Table 7.1) has been prepared as a guide to evaluate the effects of divalent and trivalent cation substitution on the A site. The variations in divalent cation size (M<Ca<Sr<Ba) can relate to the localized lattice distortion on small polaron transport and as the base for better understanding the theoretical model.

Thermal property measurements will be used to evaluate ways to increase ZT by decreasing λ. The variation in trivalent cation size (Gd<Y<La) on the A site, in addition to affecting the transport of small polarons, will change the thermal transport properties through lattice distortion. By generating localized disorder in the unit cell, increased phonon scattering may result in the desired decrease in thermal conductivity. Substitution of trivalent atoms on the B site may also increase phonon interaction and reduce λ.

Studies will also continue on the other oxide systems now being investigated and on other material systems, such as the rare-earth sulfides and oxy-sulfides. The sulfides are known to exhibit high electronic conduction with lower thermal conductivity than the chromites.[3.3] These materials are n-type conductors. The introduction of oxygen into the sulfide lattice, because of the difference in anion size, can potentially reduce the thermal conductivity without significant reduction in σ or S. The effects of oxygen in the rare-earth sulfide on the transport properties need to be studied.

Structural information using laser Raman spectroscopy will also be generated to provide determination of the effect(s) of divalent/trivalent doping on the structure and phase composition in these materials. Extension of this optical probe technique to equivalent temperatures (as high as 1800 K) associated with the electrical/transference/thermal property measurements will be assessed.

TABLE 7.1. Future Chromite Matrix Study

$ABX_3 : (A_xA_{1-x})CrO_3$

A site divalent cation substitution: effect on electrical transport properties

$Y_{0.98}Mg_{0.02}CrO_3$		$Y_{0.95}Ca_{0.05}CrO_3$
$Y_{0.90}Mg_{0.10}CrO_3$	increasing →	$Y_{0.875}Ca_{0.125}CrO_3$
$Y_{0.85}Mg_{0.15}CrO_3$		$Y_{0.85}Ca_{0.15}CrO_3$
	cation ↙	
$Y_{0.98}Sr_{0.02}CrO_3$		$Y0.99Ba_{0.01}CrO_3$
$Y_{0.95}Sr_{0.05}CrO_3$	size →	$Y_{0.98}Ba_{0.02}CrO_3$
$Y_{0.925}Sr_{0.075}CrO_3$		$Y_{0.95}Ba_{0.05}CrO_3$
$Y_{0.90}Sr_{0.1}CrO_3$		
$Y_{0.85}Sr_{0.15}CrO_3$		

A trivalent cation substitution A Site: effect on thermal/electrical transport properties

$(Y_{0.5}La_{0.5})_{0.98}Sr_{0.02}CrO_3$

$(Y_{0.5}Gd_{0.5})_{0.98}Sr_{0.02}CrO_3$

$(La_{0.5}Gd_{0.5})_{0.98}Sr_{0.02}CrO_3$

$La_{0.98}Sr_{0.02}CrO_3$

$La_{0.95}Sr_{0.05}CrO_3$

$La_{0.925}Sr_{0.075}CrO_3$

$La_{0.90}Sr_{0.10}CrO_3$

$La_{0.85}Sr_{0.15}CrO_3$

$La_{0.8}Sr_{0.2}CrO_3$

The effect of oxygen pressure on the electrical and thermal transport properties and thermodynamic stability of chromites will also be considered. Determination of variances in σ, S and mobility with decreasing oxygen partial pressure will be made on a limited number of chromite compositions.

The experimental studies will emphasize electrical and thermal transport measurements as well as some preliminary transference property measurements on selected compositions. The transference data will provide information on the mobility, of major charge carrier and using different divalent cations, the effects of unit cell strain on the mobility can also be assessed. This type of information can provide insight to the mechanism(s) of small polaron transport and scattering. Initial transference number evaluations will be made at Marquette University and will provide standards for later measurements made at Battelle.

8.0 REFERENCES

3.1 Wood, C. and D. Emin. "Refractory Materials for High-Temperature Thermoelectric Energy Conversion." Work done at Jet Propulsion Laboratory under DOE Contract No. DE-AC06-76CD P00789.

3.2 Shapiro, E. and L. R. Danielson. 1983. "Thermoelectric Properties of Non-Stoichiometric Lanthanum Sulfides." Proc. of 18th Intersociety Energy Conversion Engineering Conference. P. 249.

3.3 Taher, S. M. and J. B. Gruber. 1981. "Thermoelectric Efficiency of Rare Earth Sesquisulfides." Mat. Res. Bull., 16:1407.

3.4 Emin, D. and C. Wood. 1983. "Small-Polaron Electronic Transport in Boron Carbides." Proc. 18th Intersociety Energy Conversion Engineering Conference. P. 222.

3.5 Elsner, N. B. and G. H. Reynolds. 1983. "Present State of Boron-Carbon Thermoelectric MATERIALS." IBID, page 227.

4.1 Heikes, R. R. and R. W. Ure, Jr. 1961. Thermoelectricity: Science and Engineering, Interscience Publishers. New York, New York.

4.2 Ure, R. W. 1972. "Practical Limits to the Thermoelectric Figure of Merit-II." Energy Conversion. 12:45.

5.1 Bates, J. L. 1970. High-Temperature Thermal Conductivity of "Round-Robin" Uranium Dioxide. BNWL-1431, Battelle, Pacific Northwest Laboratories, Richland, Washington.

5.2 Parker, W. J., R. J. Jenkins, C. P. Butler, and G. L. Abbott. 1961. "Flash Method of Determining Thermal Diffusivity, Heat Capacity, and Thermal Conductivity." J. Appl. Phys., 32(9):1679-1684.

5.3 Deem, H. W. and W. D. Wood. 1962. "Flash Thermal-Diffusivity Measurements Using a Laser." Rev. Sci. Instr., 33:1107-1109.

5.4 Cowan, R. D. 1963. "Pulse Method of Measuring Thermal Diffusivity at High Temperatures." J. Appl. Phys., 34(4):926-927.

5.5 Cape, J. A. and G. W. Lehman. 1963. "Temperature and Finite Pulse-Time Effects in the Flash Method for Measuring Thermal Diffusivity." J. Appl. Phys., 34(7):1909-1913.

5.6 Taylor, R. E. and J. A. Cape. 1964. "Finite Pulse-Time Effects in Flash Diffusivity Technique." Appl. Phys. Letters, 5(10):212-213.

6.1 Bates, J. L. and D. D. Marchant. 1984. "Oxide Electrodes for High-Temperature Fuel Cells." Fossil Energy Materials Program Quarterly Progress Report - for Period Ending Dec. 31, 1983. ORNL/FMP-84-1, pp. 483-500, Oak Ridge, Tennessee.

6.2 Meadowcroft, D. B. 1969. "Properties of Strontium-Doped Lanthanum Chromite." Brit. J. Appl. Phys., Ser. 2, 2:125-1233.

6.3 Flandermeyer, B. K. et al. 1984. "Defect Structure of Mg-doped $LaCrO_3$ Model and Thermogravimetric Measurements." J. Am. Cer. Soc., 67(3):195-198.

6.4 Khattuk, C. P. and D. E. Cox. 1977. "Phase Equilibria in the $(La,Sr)CrO_3$ System." In Conference on High-Temperature Science Related to Open-Cycle, Coal-Fired MHD Systems. ANL-77-21. Argonne National Laboratory, Argonne, Illinois, p. 160-169.

6.5 Bates, J. L. and D. D. Marchant. 1984. "Oxide Electrodes for High-Temperature Fuel Cells." Fossil Energy Materials Program Quarterly Progress Report - for Period Ending Mar. 31, 1983. ORNL/FMP-84-2, pp. 457 to 463. Oak Ridge National Laboratory, Oak Ridge, Tennessee.

APPENDIX A - CALCULATED THERMOELECTRIC PROPERTY DATA

CALCULATED THERMOELECTRIC PROPERTY DATA

This appendix contains tables of electrical conductivity, (σ, sigma), thermal conductivity (λ, lambda), Seebeck coefficient (S), and dimensionless figure of merit (ZT) calculated at different temperatures (T, K) using the coefficients determined from the fitted data. Because sigma and sigma*T data were fitted separately, the calculated values are slightly different. In addition, the computer program did not print out the entire coefficient used to calculate the thermoelectric properties. There will be a difference between the properties listed in these tables and those calculated using the listed coefficients. The computer program is being revised to eliminate this problem; in the meantime, the authors will be happy to supply the coefficients used to calculate these thermoelectric properties. The properties were calculated by:

$$\log (\text{sigma}) = A + B/T$$

$$\log (\text{sigma} * T) = A + B/T$$

$$\text{lambda} = 1/(A + BT)$$

$$S = A + B*T + C*T^2 + D*T^3$$

$$Z = (S^2*\text{sigma})/\text{lambda}$$

$$ZT = [(S^2*\text{sigma})/\text{lambda})*T$$

THERMOELECTRIC PROPERTIES

MATERIAL:.11IN2O3-.89SNO2 TEMP RANGE. K

SAMPLE #:FC-56 MIN: 1060

NOTES: HIGH TEMP ELEC COND REGION MAX: 1101

PROPERTY	UNITS	COEFFICIENTS A	B	C	D	MINIMUM TEMP K	MAXIMUM TEMP K
LOG SIGMA	1/OHM-CM	3.6536	-4565.44	XXX	XXX	1060	1720
LOG SIG*T	1/OHM-CM	7.223044	-5150.11	XXX	XXX	1060	1720
LAMBDA	WATT/M-K	.042419	2.503E-4	XXX	XXX	563	1101
S	V/K	-2.25E-4	5.564E-7	-4.9E-10	1.39E-13	546	1504

CALCULATED PROPERTIES:

TEMP K	SIGMA 1/OHM-CM	SIGMA*T 1/OHM-CM	LAMBDA WATT/CM-K	S V/K	Z 1/K	Z*T	TEMP K
1000	.1225074	118.2851	.0341578	-2.30E-5	1.902E-9	1.902E-6	1000
1100	.3185680	347.6339	.0314670	-2.50E-5	6.329E-9	6.962E-6	1100
1200	.7064291	853.6549	.0291692	-2.77E-5	1.855E-8	2.226E-5	1200
1300	1.385878	1825.651	.0271842	-3.02E-5	4.653E-8	6.049E-5	1300
1400	2.469296	3502.605	.0254521	-3.18E-5	9.798E-8	1.372E-4	1400
1500	4.073567	6160.765	.0239275	-3.15E-5	1.694E-7	2.541E-4	1500
1600	6.312501	10097.71	.0225752	-2.87E-5	2.299E-7	3.678E-4	1600
1700	9.290699	15615.83	.0213677	-2.23E-5	2.169E-7	3.687E-4	1700
1800	13.09923	23007.51	.0202827	-1.17E-5	8.828E-8	1.589E-4	1800

THERMOELECTRIC PROPERTIES

MATERIAL:.11IN2O3-.89SNO2 — TEMP RANGE. K

SAMPLE #:FC-56 — MIN: 563

NOTES: LOW TEMP ELEC COND REGION — MAX: 1060

PROPERTY	UNITS	COEFFICIENTS A	B	C	D	MINIMUM TEMP K	MAXIMUM TEMP K
LOG SIGMA	1/OHM-CM	.130538	-893.921	XXX	XXX	524	1060
LOG SIG*T	1/OHM-CM	3.44047	-1210.40	XXX	XXX	524	1060
LAMBDA	WATT/M-K	.042419	2.503E-4	XXX	XXX	563	1101
S	V/K	-2.25E-4	5.564E-7	-4.9E-10	1.39E-13	546	1504

CALCULATED PROPERTIES:

TEMP K	SIGMA 1/OHM-CM	SIGMA*T 1/OHM-CM	LAMBDA WATT/CM-K	S V/K	Z 1/K	Z*T	TEMP K
500	.0220139	10.46350	.0596698	-5.28E-5	1.029E-9	5.144E-7	500
600	.0437190	26.49369	.0519149	-3.88E-5	1.267E-9	7.601E-7	600
700	.0713688	51.44369	.0459438	-2.96E-5	1.364E-9	9.548E-7	700
800	.1030711	84.62026	.0412047	-2.45E-5	1.503E-9	1.202E-6	800
900	.1371806	124.6192	.0373518	-2.26E-5	1.874E-9	1.686E-6	900
1000	.1724317	169.8531	.0341578	-2.30E-5	2.677E-9	2.677E-6	1000
1100	.2079135	218.8314	.0314670	-2.50E-5	4.131E-9	4.544E-6	1100

THERMOELECTRIC PROPERTIES

MATERIAL:.16IN2O3-.84SNO2 TEMP RANGE, K

SAMPLE #:FC-57 MIN: 1065

NOTES: HIGH TEMP ELEC COND REGION MAX: 1088

PROPERTY	UNITS	COEFFICIENTS A	B	C	D	MINIMUM TEMP K	MAXIMUM TEMP K
LOG SIGMA	1/OHM-CM	3.4776	-3255.68	XXX	XXX	1065	1729
LOG SIG*T	1/OHM-CM	7.04946	-3843.61	XXX	XXX	1065	1729
LAMBDA	WATT/M-K	.19413	1.982E-4	XXX	XXX	618	1088
S	V/K	-4.77E-4	1.317E-6	-1.21E-9	3.51E-13	651	1651

CALCULATED PROPERTIES:

TEMP K	SIGMA 1/OHM-CM	SIGMA*T 1/OHM-CM	LAMBDA WATT/CM-K	S V/K	Z 1/K	Z*T	TEMP K
1000	1.666930	1606.392	.0254865	-1.51E-5	1.493E-8	1.493E-5	1000
1100	3.295251	3591.456	.0242607	-2.04E-5	5.642E-8	6.206E-5	1100
1200	5.814750	7021.873	.0231475	-2.66E-5	1.774E-7	2.129E-4	1200
1300	9.402183	12383.35	.0221319	-3.16E-5	4.240E-7	5.512E-4	1300
1400	14.19425	20138.42	.0212018	-3.33E-5	7.431E-7	.0010404	1400
1500	20.28359	30694.06	.0203466	-2.96E-5	8.759E-7	.0013138	1500
1600	27.72032	44381.78	.0195578	-1.85E-5	4.829E-7	7.727E-4	1600

THERMOELECTRIC PROPERTIES

MATERIAL:.16IN2O3-.84SNO2 TEMP RANGE. K

SAMPLE #:FC-57 MIN: 651

NOTES: LOW TEMP ELEC COND REGION MAX: 1065

PROPERTY	UNITS	COEFFICIENTS A	B	C	D	MINIMUM TEMP K	MAXIMUM TEMP K
LOG SIGMA	1/OHM-CM	1.536696	-1242.45	XXX	XXX	606	1065
LOG SIG*T	1/OHM-CM	4.8771	-1585.00	XXX	XXX	606	1065
LAMBDA	WATT/M-K	.19413	1.982E-4	XXX	XXX	618	1088
S	V/K	-4.77E-4	1.317E-6	-1.21E-9	3.51E-13	651	1651

CALCULATED PROPERTIES:

TEMP K	SIGMA 1/OHM-CM	SIGMA*T 1/OHM-CM	LAMBDA WATT/CM-K	S V/K	Z 1/K	Z*T	TEMP K
600	.2923761	171.9643	.0319416	-4.55E-5	1.891E-8	1.135E-5	600
700	.5777819	410.0327	.0300395	-2.59E-5	1.294E-8	9.057E-6	700
800	.9630091	786.7807	.0283513	-1.58E-5	8.458E-9	6.766E-6	800
900	1.432825	1306.147	.0268426	-1.29E-5	8.846E-9	7.962E-6	900
1000	1.968990	1959.309	.0254865	-1.51E-5	1.764E-8	1.764E-5	1000
1100	2.553840	2730.195	.0242607	-2.04E-5	4.373E-8	4.810E-5	1100

THERMOELECTRIC PROPERTIES

MATERIAL:0.7IN2O3-0.3SNO2 TEMP RANGE, K

SAMPLE #:FC-97-9 MIN: 597

NOTES: MAX: 1291

PROPERTY	UNITS	COEFFICIENTS A	B	C	D	MINIMUM TEMP K	MAXIMUM TEMP K
LOG SIGMA	1/OHM-CM	2.845561	54.29334	XXX	XXX	597	1541
LOG SIG*T	1/OHM-CM	6.272814	-352.214	XXX	XXX	597	1541
LAMBDA	WATT/M-K	.21206	1.239E-4	XXX	XXX	500	1291
S	V/K	1.201E-6	-1.94E-8	-6.3E-11	4.31E-14	475	1342

CALCULATED PROPERTIES:

TEMP K	SIGMA 1/OHM-CM	SIGMA*T 1/OHM-CM	LAMBDA WATT/CM-K	S V/K	Z 1/K	Z*T	TEMP K
500	899.8032	370156.1	.0364970	-1.88E-5	8.690E-6	.0043448	500
600	863.0774	485053.5	.0349184	-2.37E-5	1.386E-5	.0083174	600
700	837.7661	588369.6	.0334707	-2.83E-5	2.003E-5	.0140242	700
800	819.2709	680057.6	.0321382	-3.23E-5	2.667E-5	.0213357	800
900	805.1685	761139.7	.0309078	-3.56E-5	3.298E-5	.0296851	900
1000	794.0616	832912.3	.0297681	-3.77E-5	3.801E-5	.0380074	1000
1100	785.0882	896641.4	.0287095	-3.86E-5	4.070E-5	.0447711	1100
1200	777.6878	953458.3	.0277236	-3.78E-5	4.013E-5	.0481525	1200
1300	771.4805	1004337.	.0268031	-3.52E-5	3.569E-5	.0464029	1300

THERMOELECTRIC PROPERTIES

MATERIAL:0.8IN2O3-0.2SNO2 — TEMP RANGE, K

SAMPLE #:FC-97-10 — MIN: 515

NOTES: — MAX: 1088

PROPERTY	UNITS	COEFFICIENTS A	B	C	D	MINIMUM TEMP K	MAXIMUM TEMP K
LOG SIGMA	1/OHM-CM	3.06061	61.02973	XXX	XXX	515	1527
LOG SIG*T	1/OHM-CM	6.511779	-374.664	XXX	XXX	515	1527
LAMBDA	WATT/M-K	.18422	-9.46E-5	XXX	XXX	468	1088
S	U/K	-1.14E-5	2.342E-8	-3.2E-11	1.18E-14	479	1433

CALCULATED PROPERTIES:

TEMP K	SIGMA 1/OHM-CM	SIGMA*T 1/OHM-CM	LAMBDA WATT/CM-K	S U/K	Z 1/K	Z*T	TEMP K
500	1522.893	578696.0	.0730247	-6.11E-6	7.780E-7	3.890E-4	500
600	1453.203	771504.7	.0784412	-6.17E-6	7.064E-7	4.238E-4	600
700	1405.385	947423.9	.0847257	-6.45E-6	6.900E-7	4.830E-4	700
800	1370.557	1105220.	.0921048	-6.86E-6	7.005E-7	5.604E-4	800
900	1344.067	1245906.	.1008919	-7.34E-6	7.175E-7	6.457E-4	900
1000	1323.243	1371244.	.1115325	-7.81E-6	7.239E-7	7.239E-4	1000
1100	1306.446	1483116.	.1246821	-8.21E-6	7.059E-7	7.765E-4	1100
1200	1292.612	1583284.	.1413468	-8.46E-6	6.541E-7	7.850E-4	1200
1300	1281.020	1673307.	.1631534	-8.49E-6	5.659E-7	7.356E-4	1300
1400	1271.167	1754534.	.1929161	-8.23E-6	4.466E-7	6.252E-4	1400
1500	1262.689	1828112.	.2359604	-7.62E-6	3.104E-7	4.655E-4	1500

THERMOELECTRIC PROPERTIES

MATERIAL:Y.98CA.02CRO3 TEMP RANGE, K

SAMPLE #:M166A MIN: 820

NOTES: MAX: 1259

PROPERTY	UNITS	COEFFICIENTS A	B	C	D	MINIMUM TEMP K	MAXIMUM TEMP K
LOG SIGMA	1/OHM-CM	.68497	-421.814	XXX	XXX	820	1559
LOG SIG*T	1/OHM-CM	4.179837	-904.814	XXX	XXX	820	1559
LAMBDA	WATT/M-K	.088764	2.464E-4	XXX	XXX	553	1758
S	V/K	7.485E-4	-9.83E-7	1.063E-9	-3.4E-13	431	1259

CALCULATED PROPERTIES:

TEMP K	SIGMA 1/OHM-CM	SIGMA*T 1/OHM-CM	LAMBDA WATT/CM-K	S V/K	Z 1/K	Z*T
800	1.437814	1118.972	.0349831	4.680E-4	9.001E-6	.0072005
900	1.645463	1494.473	.0322074	4.764E-4	1.159E-5	.0104353
1000	1.832974	1883.748	.0298397	4.877E-4	1.461E-5	.0146081
1100	2.002179	2276.558	.0277963	4.997E-4	1.799E-5	.0197859
1200	2.155056	2665.786	.0260148	5.105E-4	2.159E-5	.0259084
1300	2.293495	3046.676	.0244480	5.180E-4	2.517E-5	.0327256

THERMOELECTRIC PROPERTIES

MATERIAL:Y.9CA.1CRO3 — TEMP RANGE. K

SAMPLE #:AF05-R2 — MIN: 664

NOTES: — MAX: 1510

PROPERTY	UNITS	COEFFIICIENTS A	B	C	D	MINIMUM TEMP K	MAXIMUM TEMP K
LOG SIGMA	1/OHM-CM	.74539	-595.158	XXX	XXX	511.15	1530.65
LOG SIG*T	1/OHM-CM	4.141136	-965.596	XXX	XXX	511.15	1530.65
LAMBDA	WATT/M-K	.21522	2.849E-4	XXX	XXX	550	1510
S	V/K	5.716E-4	-8.21E-7	8.24E-10	-2.5E-13	664	1586

CALCULATED PROPERTIES:

TEMP K	SIGMA 1/OHM-CM	SIGMA*T 1/OHM-CM	LAMBDA WATT/CM-K	S V/K	Z 1/K	Z*T	TEMP K
600	.5668402	340.2587	.0258971	3.211E-4	2.256E-6	.0013538	600
700	.7855337	577.7142	.0241178	3.140E-4	3.212E-6	.0022481	700
800	1.003328	859.2922	.0225673	3.128E-4	4.351E-6	.0034806	800
900	1.213679	1170.177	.0212042	3.160E-4	5.715E-6	.0051439	900
1000	1.413294	1498.097	.0199963	3.220E-4	7.329E-6	.0073286	1000
1100	1.600802	1833.670	.0189186	3.293E-4	9.178E-6	.0100961	1100
1200	1.775928	2170.063	.0179511	3.365E-4	1.120E-5	.0134427	1200
1300	1.938994	2502.474	.0170778	3.419E-4	1.328E-5	.0172588	1300
1400	2.090631	2827.641	.0162855	3.442E-4	1.521E-5	.0212900	1400
1500	2.231610	3143.439	.0155635	3.417E-4	1.674E-5	.0251095	1500
1600	2.362743	3448.563	.0149028	3.329E-4	1.757E-5	.0281173	1600

THERMOELECTRIC PROPERTIES

MATERIAL:Y.9CA.1CRO3 TEMP RANGE, K

SAMPLE #:AF05-R1 MIN: 664

NOTES: MAX: 1510

PROPERTY	UNITS	COEFFIICIENTS A	B	C	D	MINIMUM TEMP K	MAXIMUM TEMP K
LOG SIGMA	1/OHM-CM	.74539	-595.158	XXX	XXX	511.15	1530.65
LOG SIG*T	1/OHM-CM	4.141136	-965.596	XXX	XXX	511.15	1530.65
LAMBDA	WATT/M-K	.21522	2.849E-4	XXX	XXX	550	1510
S	V/K	2.242E-4	1.883E-7	-5.0E-11	-7.7E-15	664	1586

CALCULATED PROPERTIES:

TEMP K	SIGMA 1/OHM-CM	SIGMA*T 1/OHM-CM	LAMBDA WATT/CM-K	S V/K	Z 1/K	Z*T	TEMP K
600	.5668402	340.2587	.0258971	3.175E-4	2.207E-6	.0013240	600
700	.7855337	577.7142	.0241178	3.288E-4	3.522E-6	.0024654	700
800	1.003328	859.2922	.0225673	3.388E-4	5.104E-6	.0040835	800
900	1.213679	1170.177	.0212042	3.475E-4	6.910E-6	.0062194	900
1000	1.413294	1498.097	.0199963	3.547E-4	8.891E-6	.0088906	1000
1100	1.600802	1833.670	.0189186	3.604E-4	1.099E-5	.0120902	1100
1200	1.775928	2170.063	.0179511	3.646E-4	1.315E-5	.0157846	1200
1300	1.938994	2502.474	.0170778	3.673E-4	1.532E-5	.0199131	1300
1400	2.090631	2827.641	.0162855	3.684E-4	1.742E-5	.0243873	1400
1500	2.231610	3143.439	.0155635	3.678E-4	1.939E-5	.0290920	1500
1600	2.362743	3448.563	.0149028	3.655E-4	2.118E-5	.0338863	1600

THERMOELECTRIC PROPERTIES

MATERIAL:Y.8CA.2CRO3 TEMP RANGE. K

SAMPLE #:AF06-R2 MIN: 642

NOTES: LOW TEMP ELEC COND REGION MAX: 1180

PROPERTY	UNITS	COEFFIICIENTS A	B	C	D	MINIMUM TEMP K	MAXIMUM TEMP K
LOG SIGMA	1/OHM-CM	.7555882	-560.140	XXX	XXX	515	1180
LOG SIG*T	1/OHM-CM	4.083141	-884.419	XXX	XXX	515	1180
LAMBDA	WATT/M-K	.157652	2.709E-4	XXX	XXX	528	1448
S	V/K	1.111E-4	3.332E-7	-1.8E-10	2.62E-14	642	1558

CALCULATED PROPERTIES:

TEMP K	SIGMA 1/OHM-CM	SIGMA*T 1/OHM-CM	LAMBDA WATT/CM-K	S V/K	Z 1/K	Z*T	TEMP K
600	.6637767	406.5460	.0312318	2.534E-4	1.365E-6	8.190E-4	600
700	.9023782	660.2151	.0287956	2.672E-4	2.238E-6	.0015664	700
800	1.136092	949.7676	.0267120	2.786E-4	3.301E-6	.0026409	800
900	1.358973	1260.240	.0249095	2.877E-4	4.516E-6	.0040647	900
1000	1.568370	1580.236	.0233349	2.947E-4	5.839E-6	.0058388	1000
1100	1.763479	1901.620	.0219476	2.998E-4	7.223E-6	.0079449	1100
1200	1.944487	2218.835	.0207159	3.031E-4	8.624E-6	.0103484	1200

THERMOELECTRIC PROPERTIES

MATERIAL:Y.8CA.2CR03 TEMP RANGE, K

SAMPLE #:AF06-R2 MIN: 1180

NOTES: HIGH TEMP ELEC COND REGION REGION MAX: 1448

PROPERTY	UNITS	COEFFIICIENTS A	B	C	D	MINIMUM TEMP K	MAXIMUM TEMP K
LOG SIGMA	1/OHM-CM	1.471787	-1382.14	XXX	XXX	1180	1552
LOG SIG*T	1/OHM-CM	5.039732	-1979.78	XXX	XXX	1180	1552
LAMBDA	WATT/M-K	.157652	2.709E-4	XXX	XXX	528	1448
S	V/K	1.111E-4	3.332E-7	-1.8E-10	2.62E-14	642	1558

CALCULATED PROPERTIES:

TEMP K	SIGMA 1/OHM-CM	SIGMA*T 1/OHM-CM	LAMBDA WATT/CM-K	S V/K	Z 1/K	Z*T	TEMP K
1100	1.641698	1737.531	.0219476	2.998E-4	6.724E-6	.0073963	1100
1200	2.089301	2454.233	.0207159	3.031E-4	9.266E-6	.0111191	1200
1300	2.562123	3287.190	.0196152	3.048E-4	1.213E-5	.0157721	1300
1400	3.051700	4222.833	.0186255	3.050E-4	1.524E-5	.0213322	1400
1500	3.551062	5246.615	.0177309	3.038E-4	1.849E-5	.0277318	1500

THERMOELECTRIC PROPERTIES

MATERIAL:YMG.02CR.9803

SAMPLE #:M163-164-R2

NOTES:

TEMP RANGE, K

MIN: 852

MAX: 1502

PROPERTY	UNITS	COEFFICIENTS A	B	C	D	MINIMUM TEMP K	MAXIMUM TEMP K
LOG SIGMA	1/OHM-CM	.096633	-383.882	XXX	XXX	852	1545
LOG SIG*T	1/OHM-CM	3.59304	-875.021	XXX	XXX	852	1545
LAMBDA	WATT/M-K	.215081	1.005E-4	XXX	XXX	538	1820
S	V/K	1.818E-4	3.572E-7	-2.0E-10	4.86E-14	617	1502

CALCULATED PROPERTIES:

TEMP K	SIGMA 1/OHM-CM	SIGMA*T 1/OHM-CM	LAMBDA WATT/CM-K	S V/K	Z 1/K	Z*T
800	.4137908	315.6926	.0338450	3.617E-4	1.599E-6	.0012796
900	.4678404	417.6332	.0327318	3.732E-4	1.991E-6	.0017919
1000	.5161207	522.4196	.0316896	3.833E-4	2.393E-6	.0023927
1100	.5593061	627.4322	.0307117	3.922E-4	2.801E-6	.0030811
1200	.5980418	730.8971	.0297923	4.002E-4	3.215E-6	.0038577
1300	.6329062	831.6628	.0289264	4.076E-4	3.635E-6	.0047258
1400	.6644032	929.0206	.0281094	4.147E-4	4.065E-6	.0056916
1500	.6929658	1022.570	.0273373	4.218E-4	4.511E-6	.0067663

THERMOELECTRIC PROPERTIES

MATERIAL:YMG.05CR.9503 — TEMP RANGE, K

SAMPLE #:M165-A/AF11-R1 — MIN: 754

NOTES: — MAX: 1421

PROPERTY	UNITS	COEFFICIENTS A	B	C	D	MINIMUM TEMP K	MAXIMUM TEMP K
LOG SIGMA	1/OHM-CM	.1525447	-747.130	XXX	XXX	490	1546
LOG SIG*T	1/OHM-CM	3.541645	-1109.10	XXX	XXX	490	1546
LAMBDA	WATT/M-K	.1265571	.0001948	XXX	XXX	754	1473
S	V/K	4.353E-4	-3.89E-7	5.29E-10	-1.9E-13	427	1421

CALCULATED PROPERTIES:

TEMP K	SIGMA 1/OHM-CM	SIGMA*T 1/OHM-CM	LAMBDA WATT/CM-K	S V/K	Z 1/K	Z*T
500	.0455286	21.05904	.0446514	3.497E-4	1.247E-7	6.233E-5
600	.0807844	49.33324	.0410784	3.520E-4	2.437E-7	1.462E-4
700	.1216790	90.61744	.0380348	3.583E-4	4.107E-7	2.875E-4
800	.1654367	142.9769	.0354111	3.674E-4	6.305E-7	5.044E-4
900	.2100874	203.8487	.0331261	3.781E-4	9.065E-7	8.159E-4
1000	.2543399	270.7333	.0311180	3.893E-4	1.239E-6	.0012390
1100	.2973962	341.4831	.0293395	4.001E-4	1.622E-6	.0017846
1200	.3387944	414.3737	.0277533	4.091E-4	2.043E-6	.0024517
1300	.3782937	488.0772	.0263298	4.154E-4	2.479E-6	.0032222
1400	.4157960	561.6014	.0250453	4.177E-4	2.897E-6	.0040552

THERMOELECTRIC PROPERTIES

MATERIAL:Y.9SR.1CRO3 TEMP RANGE, K

SAMPLE #:AF01-R1 MIN: 1283

NOTES: HIGH TEMP ELEC COND REGION MAX: 990

PROPERTY	UNITS	COEFFIICIENTS A	B	C	D	MINIMUM TEMP K	MAXIMUM TEMP K
LOG SIGMA	1/OHM-CM	1.128205	-1665.82	XXX	XXX	1283	1544
LOG SIG*T	1/OHM-CM	4.711723	-2276.52	XXX	XXX	1283	1544
LAMBDA	WATT/M-K	.135526	3.119E-4	XXX	XXX	608	990
S	V/K	-.001359	5.080E-6	-4.15E-9	9.95E-13	708	1538

CALCULATED PROPERTIES:

TEMP K	SIGMA 1/OHM-CM	SIGMA*T 1/OHM-CM	LAMBDA WATT/CM-K	S V/K	Z 1/K	Z*T	TEMP K
1200	.5495647	652.5640	.0196175	4.760E-4	6.346E-6	.0076155	1200
1300	.7027525	913.1747	.0184865	4.122E-4	6.459E-6	.0083972	1300
1400	.8676232	1217.972	.0174788	3.430E-4	5.839E-6	.0081752	1400
1500	1.041492	1563.303	.0165754	2.742E-4	4.726E-6	.0070888	1500
1600	1.221984	1944.904	.0157607	2.120E-4	3.484E-6	.0055740	1600

THERMOELECTRIC PROPERTIES

MATERIAL:Y.9SR.1CRO3 TEMP RANGE. K

SAMPLE #:AF01-R1 MIN: 708

NOTES: LOW TEMP ELEC COND REGION MAX: 990

PROPERTY	UNITS	COEFFIICIENTS A	B	C	D	MINIMUM TEMP K	MAXIMUM TEMP K
LOG SIGMA	1/OHM-CM	.2152999	-554.555	XXX	XXX	565	1283
LOG SIG*T	1/OHM-CM	3.583162	-912.419	XXX	XXX	565	1283
LAMBDA	WATT/M-K	.135526	3.119E-4	XXX	XXX	608	990
S	V/K	-.001359	5.080E-6	-4.15E-9	9.95E-13	708	1538

CALCULATED PROPERTIES:

TEMP K	SIGMA 1/OHM-CM	SIGMA*T 1/OHM-CM	LAMBDA WATT/CM-K	S V/K	Z 1/K	Z*T	TEMP K
700	.2648983	190.4174	.0282627	5.037E-4	2.378E-6	.001664	700
800	.3327414	277.1012	.0259735	5.568E-4	3.972E-6	.003177	800
900	.3973088	370.9910	.0240273	5.747E-4	5.461E-6	.0049147	900
1000	.4578734	468.5363	.0223524	5.632E-4	6.497E-6	.006495	1000

THERMOELECTRIC PROPERTIES

MATERIAL:Y.8SR.2CR03 TEMP RANGE. K

SAMPLE #:AF02-R1 MIN: 1172

NOTES: HIGH TEMP ELEC COND REGION MAX: 1484

PROPERTY	UNITS	COEFFIICIENTS A	B	C	D	MINIMUM TEMP K	MAXIMUM TEMP K
LOG SIGMA	1/OHM-CM	2.178193	-3416.62	XXX	XXX	1172	1538
LOG SIG*T	1/OHM-CM	5.742102	-3998.93	XXX	XXX	1172	1538
LAMBDA	WATT/M-K	.14491	1.983E-4	XXX	XXX	426	1484
S	V/K	3.021E-4	9.662E-8	-2.1E-10	1.15E-13	624	1509

CALCULATED PROPERTIES:

TEMP K	SIGMA 1/OHM-CM	SIGMA*T 1/OHM-CM	LAMBDA WATT/CM-K	S V/K	Z 1/K	Z*T	TEMP K
1100	.1180793	127.8523	.0275435	3.042E-4	3.968E-7	4.365E-4	1100
1200	.2142934	256.8372	.0261169	3.107E-4	7.920E-7	9.504E-4	1200
1300	.3548321	463.4466	.0248308	3.212E-4	1.474E-6	.0019162	1300
1400	.5467004	768.6370	.0236654	3.364E-4	2.614E-6	.0036594	1400
1500	.7951436	1191.644	.0226045	3.570E-4	4.483E-6	.0067248	1500

THERMOELECTRIC PROPERTIES

MATERIAL:Y.8SR.2CR03 TEMP RANGE. K

SAMPLE #:AF02-R1 MIN: 624

NOTES: LOW TEMP ELEC COND REGION MAX: 1172

PROPERTY	UNITS	COEFFIICIENTS A	B	C	D	MINIMUM TEMP K	MAXIMUM TEMP K
LOG SIGMA	1/OHM-CM	-.046505	-738.775	XXX	XXX	497	1172
LOG SIG*T	1/OHM-CM	3.261545	-1048.91	XXX	XXX	497	1172
LAMBDA	WATT/M-K	.14491	1.983E-4	XXX	XXX	426	1484
S	V/K	3.021E-4	9.662E-8	-2.1E-10	1.15E-13	624	1509

CALCULATED PROPERTIES:

TEMP K	SIGMA 1/OHM-CM	SIGMA*T 1/OHM-CM	LAMBDA WATT/CM-K	S V/K	Z 1/K	Z*T	TEMP K
600	.0527478	32.61045	.0378929	3.083E-4	1.323E-7	7.940E-5	600
700	.0790866	57.95594	.0352443	3.050E-4	2.087E-7	1.461E-4	700
800	.1071585	89.20801	.0329418	3.022E-4	2.971E-7	2.376E-4	800
900	.1357170	124.7631	.0309217	3.007E-4	3.968E-7	3.571E-4	900
1000	.1639534	163.1669	.0291350	3.011E-4	5.103E-7	5.103E-4	1000
1100	.1913735	203.2300	.0275435	3.042E-4	6.431E-7	7.074E-4	1100
1200	.2176955	244.0343	.0261169	3.107E-4	8.046E-7	9.655E-4	1200

THERMOELECTRIC PROPERTIES

MATERIAL:.433IN2O3-.036Y2O3-.035TB4O7-.466HFO2

SAMPLE #:MMM

NOTES:

TEMP RANGE, K
MIN: 839
MAX: 1353

PROPERTY	UNITS	COEFFICIENTS A	B	C	D	MINIMUM TEMP K	MAXIMUM TEMP K
LOG SIGMA	1/OHM-CM	3.365346	-2128.89	XXX	XXX	839	1555
LOG SIG*T	1/OHM-CM	6.856641	-2613.76	XXX	XXX	839	1555
LAMBDA	WATT/M-K	.27156	3.089E-5	XXX	XXX	585	1526
S	V/K	3.930E-5	-2.38E-7	1.67E-10	-3.0E-14	451	1353

CALCULATED PROPERTIES:

TEMP K	SIGMA 1/OHM-CM	SIGMA*T 1/OHM-CM	LAMBDA WATT/CM-K	S V/K	Z 1/K	Z*T	TEMP K
800	5.060939	3885.406	.0337530	-5.96E-5	5.324E-7	4.259E-4	800
900	9.997939	8963.120	.0334047	-6.15E-5	1.133E-6	.0010201	900
1000	17.23669	17493.53	.0330635	-6.18E-5	1.990E-6	.0019900	1000
1100	26.91470	30233.77	.0327293	-6.05E-5	3.010E-6	.0033112	1100
1200	39.01838	47698.50	.0324017	-5.79E-5	4.033E-6	.0048400	1200
1300	53.42403	70154.19	.0320806	-5.41E-5	4.870E-6	.0063315	1300
1400	69.93728	97648.83	.0317659	-4.93E-5	5.352E-6	.0074923	1400

THERMOELECTRIC PROPERTIES

MATERIAL:.20IN2O3-.033YB2O3-.20PRO2-.467HFO2 TEMP RANGE, K

SAMPLE #:LLL MIN: 543

NOTES: HIGH TEMPERATURE ELEC COND REGION MAX: 1372

PROPERTY	UNITS	COEFFICIENTS A	B	C	D	MINIMUM TEMP K	MAXIMUM TEMP K
LOG SIGMA	1/OHM-CM	2.48548	-2683.73	XXX	XXX	507	1503
LOG SIG*T	1/OHM-CM	5.975438	-3167.62	XXX	XXX	507	1503
LAMBDA	WATT/M-K	.282782	-1.31E-5	XXX	XXX	543	1556
S	V/K	6.960E-5	-3.98E-7	3.38E-10	-8.4E-14	426	1372

CALCULATED PROPERTIES:

TEMP K	SIGMA 1/OHM-CM	SIGMA*T 1/OHM-CM	LAMBDA WATT/CM-K	S V/K	Z 1/K	Z*T	TEMP K
500	.0013122	.4367084	.0362039	-5.57E-5	1.12E-10	5.615E-8	500
600	.0102942	4.966677	.0363769	-6.60E-5	1.231E-9	7.388E-7	600
700	.0448308	28.20083	.0365516	-7.25E-5	6.450E-9	4.515E-6	700
800	.1351495	103.7311	.0367279	-7.58E-5	2.116E-8	1.693E-5	800
900	.3188269	285.6647	.0369060	-7.64E-5	5.041E-8	4.537E-5	900
1000	.6335012	642.4137	.0370858	-7.47E-5	9.535E-8	9.535E-5	1000
1100	1.111023	1246.753	.0372674	-7.13E-5	1.515E-7	1.667E-4	1100
1200	1.774337	2166.466	.0374507	-6.66E-5	2.103E-7	2.524E-4	1200
1300	2.636758	3457.839	.0376359	-6.12E-5	2.626E-7	3.414E-4	1300
1400	3.702782	5162.380	.0378229	-5.56E-5	3.024E-7	4.234E-4	1400

THERMOELECTRIC PROPERTIES

MATERIAL:.20IN2O3-.033YB2O3-.20PRO2-.467HFO2 TEMP RANGE. K

SAMPLE #:LLL MIN: 543

NOTES: LOW TEMPERATURE ELEC COND REGION MAX: 507

PROPERTY	UNITS	COEFFICIENTS A	B	C	D	MINIMUM TEMP K	MAXIMUM TEMP K
LOG SIGMA	1/OHM-CM	-.073844	-533.435	XXX	XXX	477	507
LOG SIG*T	1/OHM-CM	3.159815	-799.418	XXX	XXX	477	507
LAMBDA	WATT/M-K	.282782	-1.31E-5	XXX	XXX	543	1556
S	V/K	6.960E-5	-3.98E-7	3.38E-10	-8.4E-14	426	1372

CALCULATED PROPERTIES:

TEMP K	SIGMA 1/OHM-CM	SIGMA*T 1/OHM-CM	LAMBDA WATT/CM-K	S V/K	Z 1/K	Z*T	TEMP K
400	.0391354	14.49677	.0360325	-4.11E-5	1.836E-9	7.344E-7	400
500	.0723247	36.38983	.0362039	-5.57E-5	6.190E-9	3.095E-6	500

THERMOELECTRIC PROPERTIES

MATERIAL:LA.9SR.1MNO3 TEMP RANGE. K

SAMPLE #:WLM-1 MIN: 696

NOTES: MAX: 1025

PROPERTY	UNITS	COEFFICIENTS A	B	C	D	MINIMUM TEMP K	MAXIMUM TEMP K
LOG SIGMA	1/OHM-CM	2.0954	18.15841	XXX	XXX	696	1223
LOG SIG*T	1/OHM-CM	5.620266	-509.603	XXX	XXX	696	1223
LAMBDA	WATT/M-K	.640322	-2.46E-4	XXX	XXX	490	1025
S	V/K	3.400E-5	-3.99E-8	3.10E-11	-3.3E-15	473	1373

CALCULATED PROPERTIES:

TEMP K	SIGMA 1/OHM-CM	SIGMA*T 1/OHM-CM	LAMBDA WATT/CM-K	S V/K	Z 1/K	Z*T	TEMP K
600	133.5562	59010.20	.0202968	2.053E-5	2.774E-6	.0016642	600
700	132.2332	78029.93	.0213637	2.015E-5	2.514E-6	.0017598	700
800	131.2496	96219.22	.0225491	2.026E-5	2.388E-6	.0019105	800
900	130.4896	113250.5	.0238737	2.082E-5	2.369E-6	.0021318	900
1000	129.8848	129021.7	.0253636	2.182E-5	2.438E-6	.0024379	1000
1100	129.3921	143545.7	.0270519	2.324E-5	2.583E-6	.0028417	1100
1200	128.9829	156890.5	.0289809	2.506E-5	2.795E-6	.0033543	1200
1300	128.6376	169146.7	.0312062	2.726E-5	3.064E-6	.0039826	1300

APPENDIX B - NOVEL APPARATUS FOR MEASUREMENT OF SEEBECK COEFFICIENT

APPENDIX B

DRAFT

Novel Apparatus for Measurement of Seebeck Coefficient

J.E. Garnier* and J.L. Bates*+

Summary

A novel experimental apparatus has been developed for the measurement of the high temperature, absolute Seebeck coefficient in materials. The automated, computerized technique utilizes a multiprobe sensor arrangement with vertical specimen geometry to provide for accurate, rapid Seebeck determination while minimizing potential errors associated with non-isothermal specimen heating. An internal adjustable radial heater allows Seebeck values to be determined over a range of temperature gradients from 10 to 150 K. This capability combined with environmental enclosure allows a wide range of specimen temperature and atmospheric conditions to be achieved. A discussion of determinate and indeterminate errors associated with the apparatus and measurement is made. The 3 sigma uncertainty in Seebeck coefficient is found to be 2.8% or less.

* Battelle Pacific Northwest Laboratories, Richland, WA 99352
+ Member of the American Ceramic Society

I. Introduction

The Seebeck effect results in the conversion of thermal energy into electrical energy via the transport of electrical carriers (electrons/holes/ions) induced by the presence of a temperature gradient. A novel experimental apparatus was developed as part of AFOSR and DOE sponsored program for measuring the Seebeck coefficient (S) of potential thermoelectric and fuel cell materials. The apparatus developed has been found to be a simple, yet precise means, for measuring the absolute Seebeck coefficient. The determinant and indeterminant errors associated with the apparatus were made. Some results for oxide ceramics are discussed.

II. Apparatus Description

The Seebeck coefficient (S) is a local transport property measurement[1], and is determined by applying a temperature difference (ΔT) between the ends of a test specimen (rectangular bar shaped) which gives rise to a potential difference (ΔV) by virtue of the net diffusional flux of charge carriers (electrons/holes/ions) from the hot to cold temperature regions along the length of the specimen. The Seebeck coefficient is thus, by definition, given as

$$S \equiv - \lim_{\Delta T \to 0} \frac{(\Delta V)}{(\Delta T)} \quad ; \quad \bar{T} = \frac{T_{Hot} - T_{Cold}}{2}$$

wherein, the negative sign is required by convention to ensure that the sign of S and the majority charge carrier agrees.[2] It is assumed that $\delta S/\delta T$ is

approximately temperature-independent; and, that maintaining the ΔT across the specimen constant for different temperature conditions does not result in compositional gradient effects above and below T. Thus, the Seebeck coefficient for a material can be determined by making several temperature gradient and corresponding emf measurements about each T of interest. However, there are some experimental difficulties generally associated with Seebeck coefficient measurements. These include the presence of non-isothermal conditions in the cross section of the sample, the measurement of temperatures and emf that often require contact of metal leads to the sample, the chemical interaction of other materials with the sample, the control and generation of small as well as large temperature gradients and the length of time required for measurements and assessment of errors. The Seebeck coefficient technique described in the paper was developed to address these difficulties so as to allow high-temperature, absolute Seebeck coefficient measurements.

The experimental technique is illustrated in Figure (1) where four thermocouple/emf probes are located at four different regions along the length of the specimen bar. With the sample at thermal equilibrium, the multi-probe arrangement allows determination of six (ΔT, ΔV) values about T_a from which the absolute Seebeck coefficient is determined as the slope of ΔV versus ΔT.

The detail of the Seebeck apparatus is shown in Figure 2. The test specimen is placed in a vertical specimen geometry which provides a necessary radial and isothermal heating geometry along the axial length of the specimen. Non-isothermal radial specimen heating can make theoretical interpretation of test results difficult at best by introducing bias voltages into the measurement,[3] especially when more than one type of charge carrier is present. Four

temperature sensors (Pt versus Pt + 10% Rh thermocouples) are placed in contact with the specimen with a horizontal input geometry to minimize temperature errors associated with thermal shunting along the thermocouple wire.[4,5,6] The Pt leads of each sensor are also used as the voltage probe leadout wires.

The four alumina thermocouple tubes also provide for specimen support. The thermocouple wires are brought to the sample in Al_2O_3 thermocouple tubes and exit 90° through the Al_2O_3 wall, with the thermocouple bead formed outside the tube. The exit of the thermocouple wires and the bead are staggered so that they contact the sample at uniform distances along the sample length and on different sides of the sample bar or cylinder. Four additional Al_2O_3 rods with a Pt ring are placed parallel to the thermocouple tubes along the sample length to assist position the sample vertical to the Al_2O_3 tubes and to ensure a good contact of all thermocouples with the sample.

The eight Al_2O_3 tubes and rods extend out of the hot zone of the furnace and are fixed in metal fixture through which the wire leads are passed. A ceramic slip ring is inserted over the the top of the four Al_2O_3 tubes and four Al_2O_3 rods. With the sample placed in position with the thermocouples in contact, this ring provides a uniform tension of the sensor beads with the specimen without the use of bonding or metal plating. This arrangement also provides for thermal expansion effects during heating and cooling cycles. Only the Pt thermocouples are in contact with the sample.

The thermal gradient across the specimen is provided by a non-inductively wound Pt heater wound on an Al_2O_3 tube. This auxiliary inner heater fits over the Al_2O_3 tube-sample assembly and can be adjusted up or down to provide the desired thermal gradient. By simple adjustment of the heater location relative to the sample, a temperature gradients from 10 to 150 degrees K can be maintained. Typically, the ΔT range from 25 to 35 degrees K.

The specimen, sensor and internal heater assembly are inserted vertically into an Al_2O_3 muffle tube that is positioned in a resistance furnace for heating up to 1823K. Atmospheric control is provided by pre-analyzed gas inside the axial length of the outer muffle tube. Thus the oxygen partial pressure can be controlled up to approximately 2000 mm pressure.

Either parallel-pipeds or right cylinders can be used as samples and the sample length can vary. No holes or insets are machined into the specimen. The sample size presently uses rectangular bars 3.8-cm long and 3- mm square. However, the size may vary in cross section, but large size changes would require appropriate changes to the bottom metal retainer and upper slip ring dimensions. Shorter specimen lengths can also be used, but depending upon the distance between the distance between probes, less than the four thermocouples may be used.

The four thermocouples are calibrated in place under isothermal conditions using a reference thermocouple calibrated to the melting point of gold. A separate thermocouple is used to control the ambient temperature of the furnace. The furnace is separately controlled as is the inner heater. However, both can be directly controlled by computer if desired.

A schematic of the data acquisition system is shown in Figure 3. The temperature sensor and voltage probe leads are hard-wired in a pre-determined sequence to a multiplex scanner switch box which is computer addressable. Under graphic computer control (HP-9836) a sequence of six (ΔV, ΔT) measurements (see Figure 1) are switched through a digital microvolt meter whose output is read by the host computer and stored for later analysis. This measurement process requires about 5 seconds and allows repeated cross checks on the data to be performed (i.e. reproducibility, standard deviation, temperature change, etc.) for each determined value of Seebeck coefficient measured. The graphic computer then calculates the necessary corrections to the raw data which includes: referencing each thermocouple emf to the National Bureau of Standards; correction of voltage lead wires for induced emf effects arising from the Pt lead wires being in a temperature gradient. Existing literature[7,8,9] information for the Seebeck coefficient of Pt is used in this correction. This latter procedure allows elimination of individual Pt lead wire biasing effects that result from initial chemical compositional variances in the Pt wires and a means of recalibrating for Pt wire aging effects.

The graphic computer functions in conjunction with a pre-programmed time-temperature furnace controller which adjusts the outer furnace to follow a step-wise temperature heating/cooling cycle or constant rate in temperature change.

III. Experimental Uncertainties

The errors involved in the Seebeck transport property measurement can be divided into two areas for assessment --- indeterminate and determinant errors. Indeterminate errors occur from system variation from assumed boundary conditions and other sources that can often be difficult to recognize and eliminate and measure. Determinate errors are associated with the measurement of quantities used in calculating the particular property of interest (i.e. Seebeck coefficient). These errors can be assessed by the inaccuracies associated with instruments used to measure (temperature sensors, voltage leads, multiplex scanner, microvoltmeter, computer) and to reproduce these quantities.

The indeterminate errors in the measurement of the Seebeck coefficient are listed in Table 1. Of the postulated indeterminate errors the largest potential source of error is considered to be in the absolute value of the Seebeck coefficient. To date no NBS reference standards[10] exist to allow assessment of the magnitude of this potential bias error. However, since the Seebeck values of promising thermoelectric materials are in the range of ±100 to 1000 μV/K this bias effect of 5 μV absolute is on the order of 5% or less.

The determinate errors associated with the measurement of various quantities used in determining the Seebeck coefficient are listed in Table 2.

Table 1. Indeterminate Errors in Seebeck Measurement

Indeterminate Error	Comments
Radial temperature gradients within specimen -- bias voltages/non-linear temperature gradients	Vertical specimen orientation and radial heating geometry minimizes this effect.
Thermal shunting by Pt/Pt - 10% Rh leads	All temperature sensor leads have initial horizontal orientation away from the specimen within their respective radial temperature zones
Thermal and Electrical contact with specimen surface	Contact between each thermocouple bead and specimen is assured by design. Uniform pressure of contact by each bead to specimen surface is maintained by simple slip ring assembly. Cooling/heating thermal expansion effects on uniformity of bead contact pressure are eliminated by design.
Absolute value of determined Seebeck coefficient	All measured specimen Seebeck coefficients are referenced to a Pt standard specimen whose chemical composition corresponds to literature reported "reference grade Pt standards." An error bias up to 5 μV absolute (within the reported literature[7,8,9] uncertainty) is possible.

Table 2. Determinate Errors in Seebeck Measurement

Determinate Error	Equivalent μV	Total Seebeck Statistical Error
° Voltage gradient		
scanner switch	< 1	3 Sigma S = ± 2.8%
digital voltmeter	± 1	
reproducibility	± 1	Origin intercept < 2.0%
° Temp. Gradient		
measurement	± 2	
absolute value	10	
° Temperature		
thermocouple deviation	10	

Using the method of Kline and McClintock[11] [Mech. Engs. 75:3, Jan. 1953] for estimating the uncertainty in experiments, the total 3σ error is estimated to be ± 2.8% which translates to a ΔV versus ΔT origin intercept error ($\Delta T_{\Delta V \to 0}/\Delta T_{max}$) of < 2%. Table 2 and Figure 4-6 summarize the results of these calculations.

Example of Test Results

The determinate uncertainties listed in Table 2 along with time variations in T_{avg} are used in the controlling computer program to determine if isothermal conditions within the test apparatus have been achieved. When the rate of change in T_{avg} is less than 2 K/minute, the origin intercept errors are <2%, reproducible emf measurements (±1 μv) are observed when these conditions occur during measurements. The computer then stores the raw/corrected/computed information for later analysis.

An example of computed information is given in Table 4. The upper right hand plot is the absolute temperature variation versus distance across the test specimen. The upper left figure is the ΔV versus ΔT data corrected for the Pt lead wires. The absolute Seebeck coefficient is determined by an un-weighted, least squares analysis given the six ΔV, ΔT pairs of data. This computed value is preferred over using the origin 0,0 (ΔV, ΔT) as either a datum point itself (Seeorg 2)[12] or forcing a fit through the origin 0,0 (Seeorg 1) as it may lead to a possible biasing of results especially if more than one charge carrier is active or a heterogeneous concentration of ionized impurities are present in the specimen. Further examples of test results are shown in Figures 7 and 8 where S vs T and S vs composition results are shown for a variety of In_2O_3 - SnO_2 compound specimens.

V. Conclusions

To be written.

VI. References

To be included later.

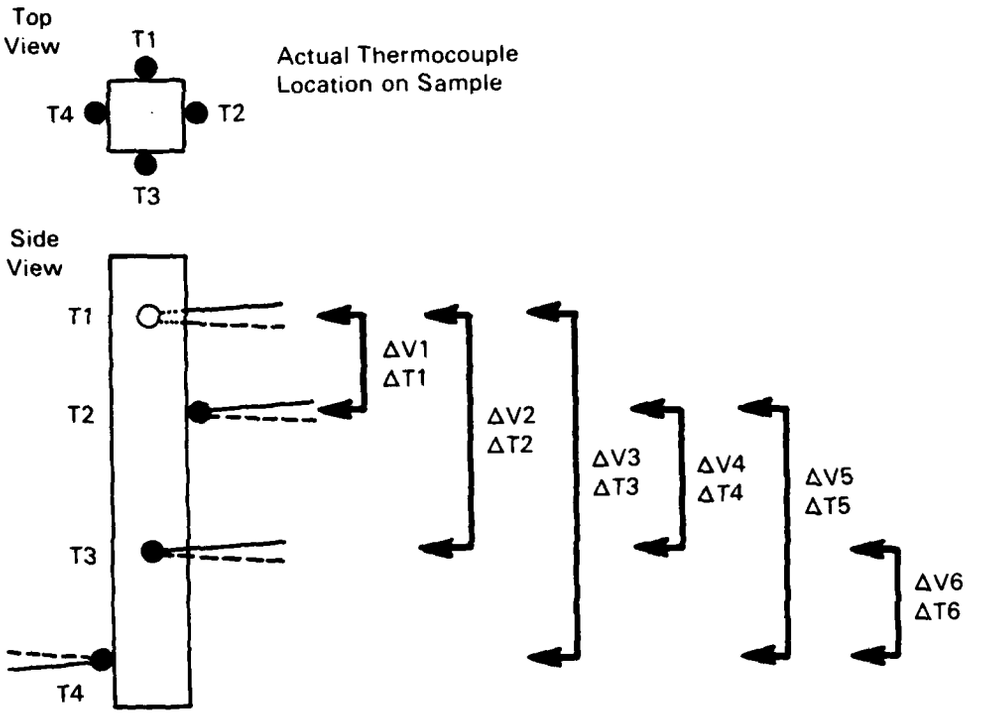

$$T_{AVG} = \frac{1}{4} \sum_{i=1}^{4} T_i$$

ΔT's: ΔT1 = T1-T2; Etc.

ΔV's: Measured Between Pt Leg TC

Seebeck
Coefficient: Slope of ΔV vs ΔT

FIGURE B.1. Multiprobe Arrangement of Seebeck Apparatus

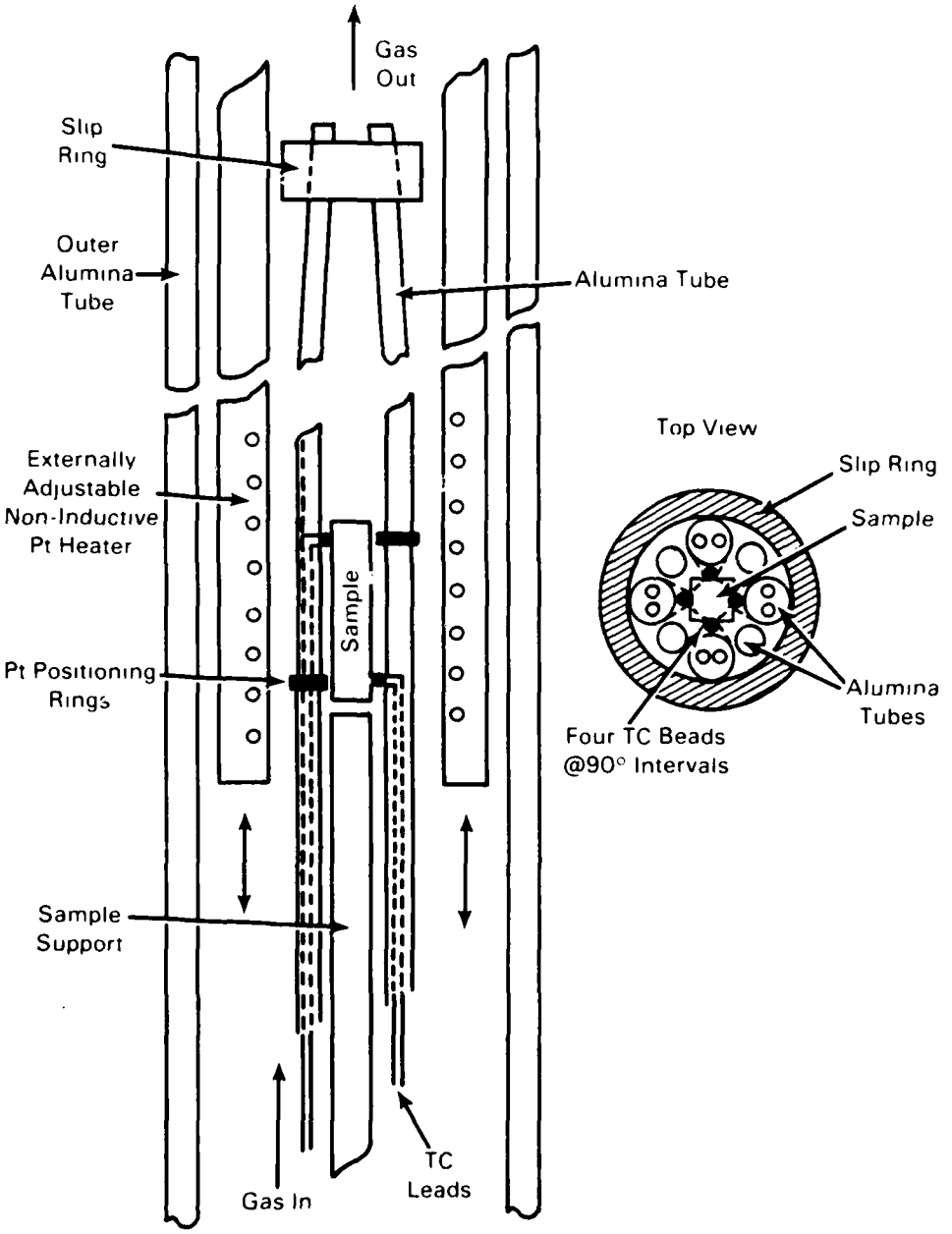

FIGURE B.2. Interior Details of Thermoelectric Power Apparatus

AD-A150 167 ELECTRICAL AND THERMAL TRANSPORT PROPERTY STUDIES OF HIGH-TEMPERATURE THE.. (U) BATTELLE PACIFIC NORTHWEST LAB RICHLAND WA J L BATES ET AL. JUL 84 2/2

UNCLASSIFIED AFOSR-TR-84-1210 F49620-83-C-0109 F/G 11/2 NL

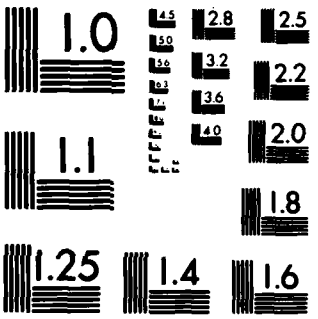

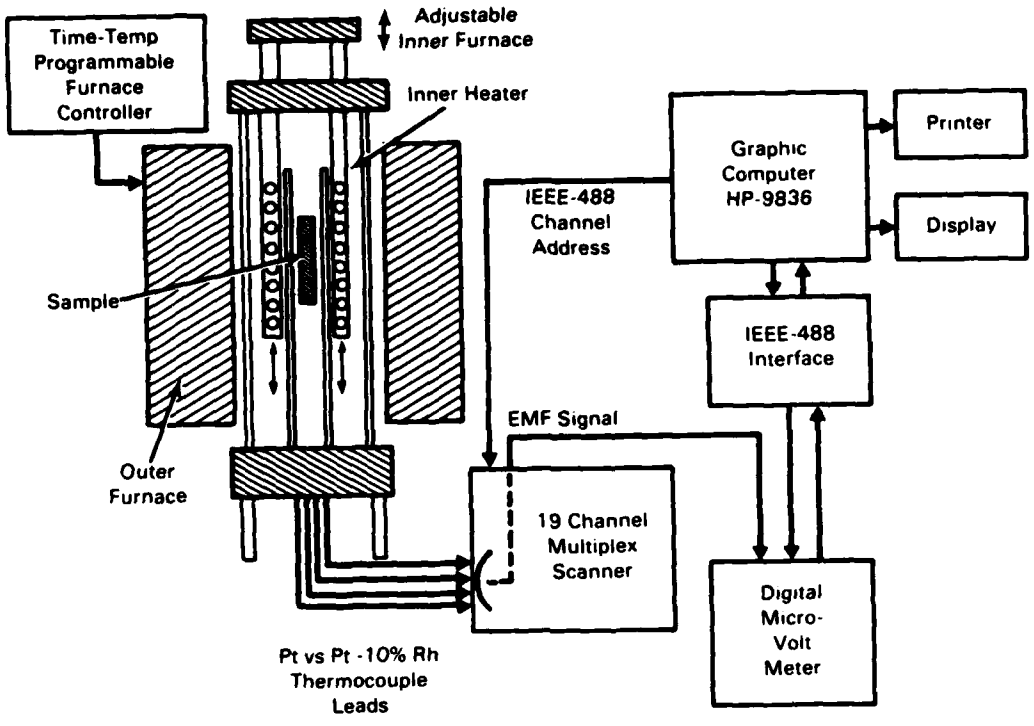

FIGURE B.3. Schematic of Data Acquisition System

TABLE B.2. Assessment of Experimental Error

Standard Deviations[1]

$$3\sigma_{\Delta V} = 3\sqrt{(\sigma_{V1})^2} = 6\mu V \qquad 3\sigma_{\Delta T} = 3\sqrt{(\sigma_{T_1})^2 + (\sigma_{T_2})^2} = 8.48\mu V \text{ or } \pm 0.85°C$$

$$3\sigma_s \equiv W_s = \left[\sum_{i=1}^{m}\left(\frac{\alpha S}{\alpha J_i}\ Wi\right)^2\right]^{1/2}$$

$$= \frac{1}{\Delta T}\left(\frac{\Delta V^2}{\Delta T^2} \bullet W_{\Delta T}^2 + \frac{W_{\Delta V}{}^2}{1}\right)^{1/2}$$

$$= \frac{1}{\Delta T}\left(\frac{\Delta V^2}{\Delta T^2} \bullet 7.191\times10^{-11} + 3.6\times10^{-11}\right)^{1/2}$$

Where ΔT and ΔV are Variable Quantities; $W_{\Delta T} = 0.85°C$; $W_{\Delta V} = 6\mu V$

[1]Based on Kline and McClintock, "Describing Uncertainties in Single Sample Experiments." Mech. Engs 75:3, January 1953.

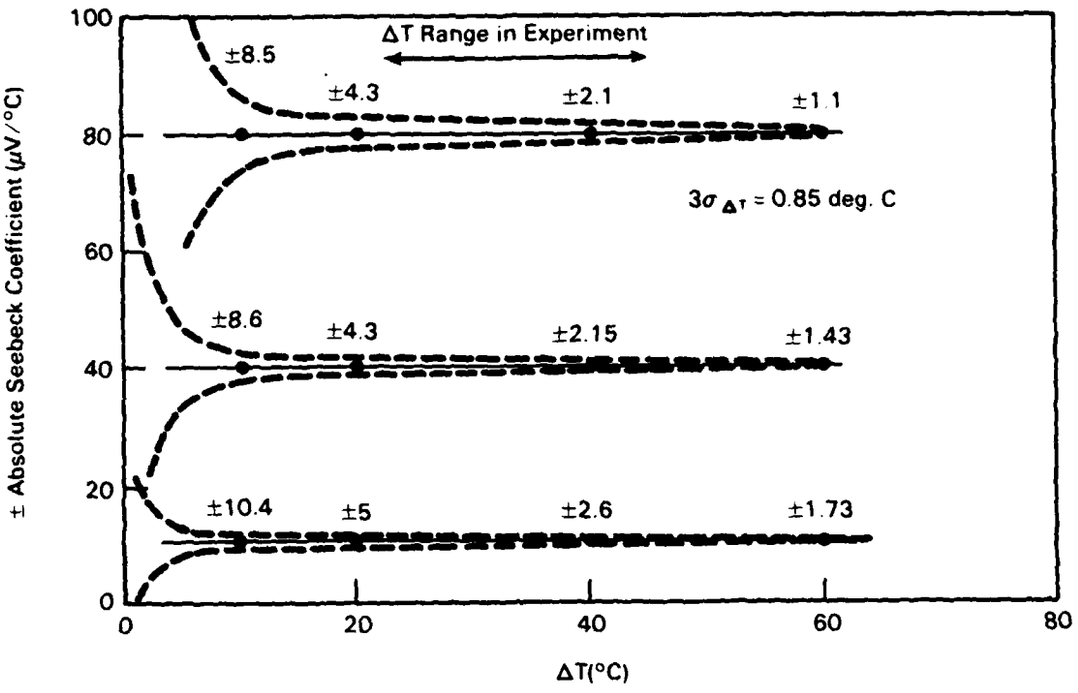

FIGURE B.4. 3σ Uncertainty Error Bars for Seebeck Coeeficient Versus ΔT

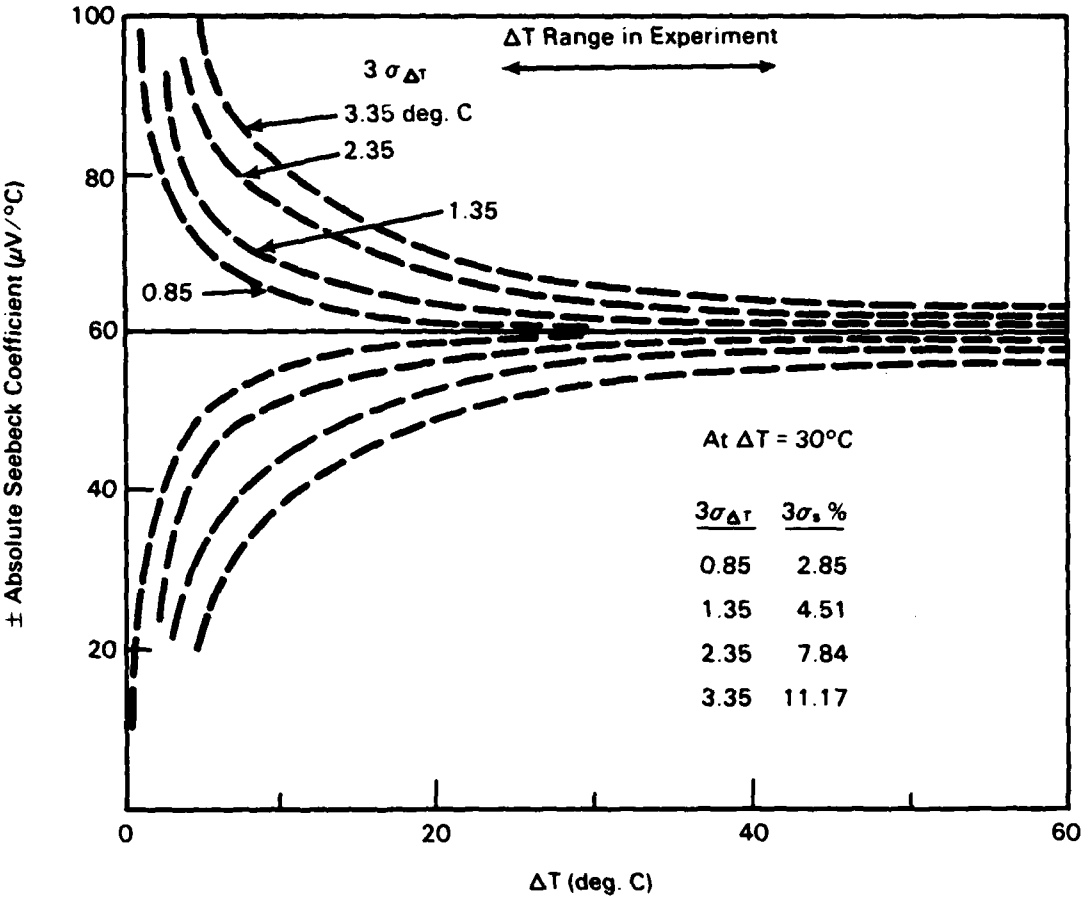

FIGURE B.5. Effect of 3σ (ΔT) Variation on 3σ (S)

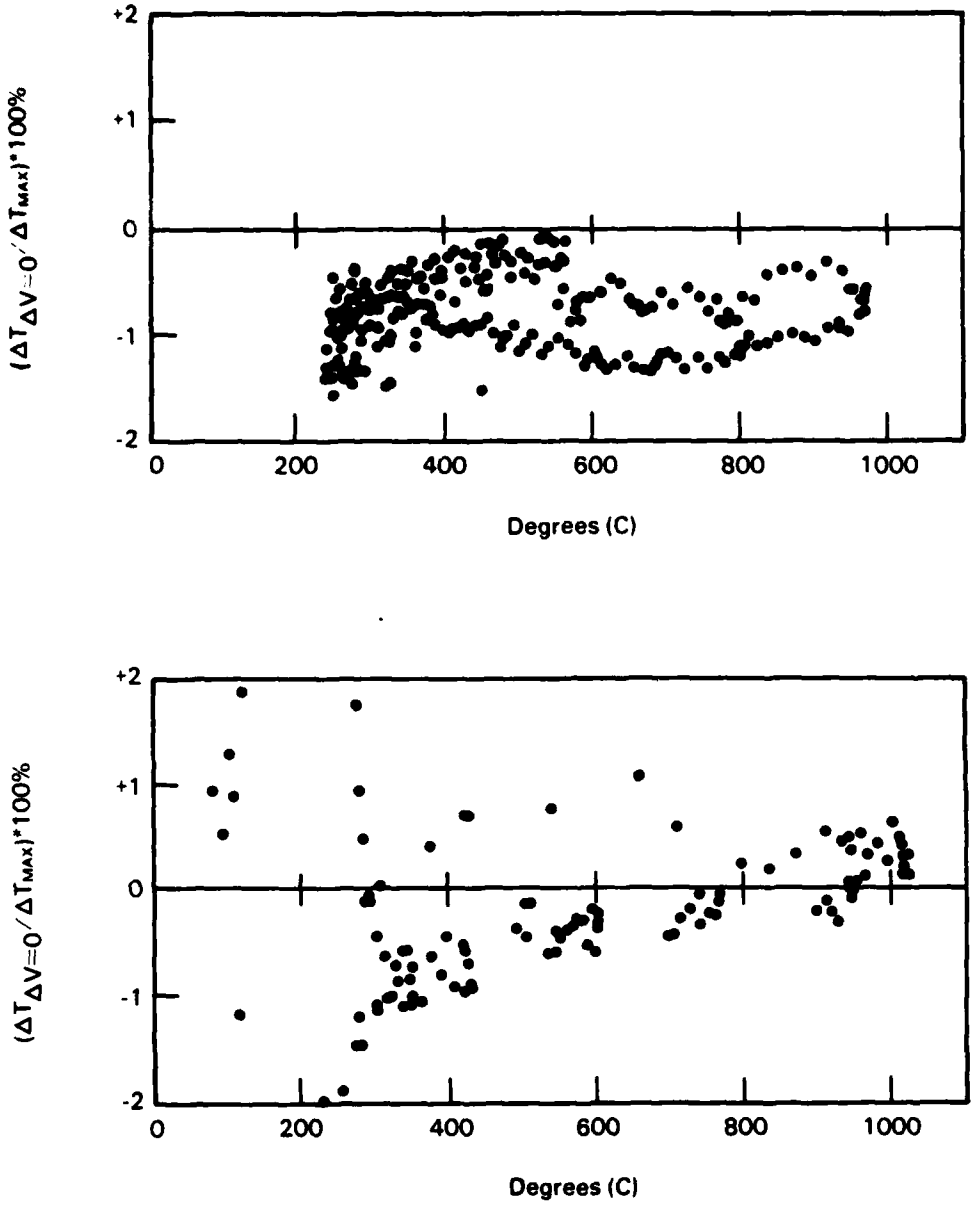

FIGURE B.6. Origin Intercept Error Versus Temperature

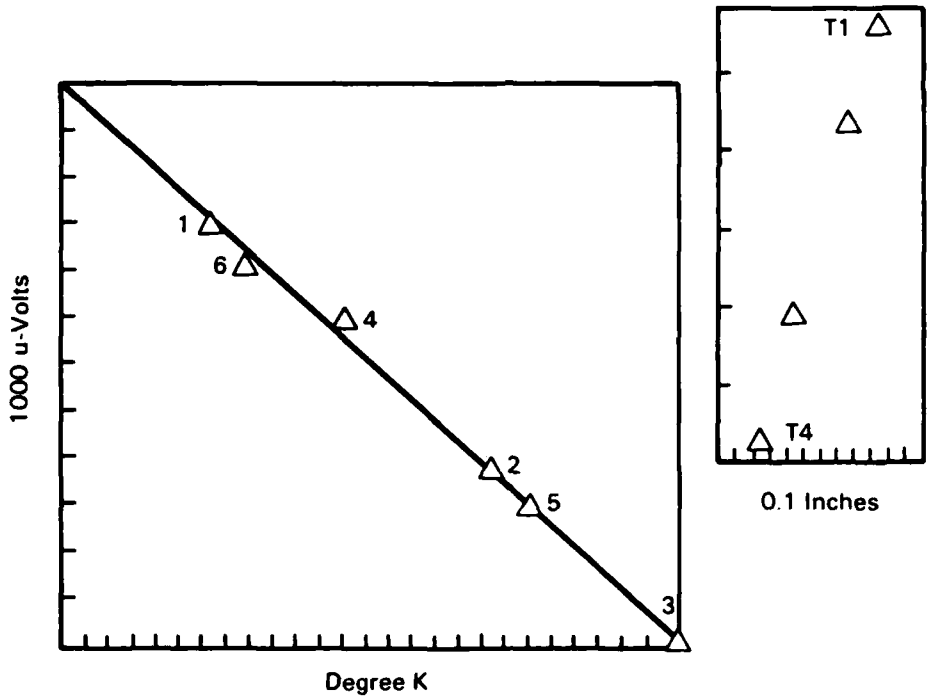

Sample #AF01 - 2R2 31 May 1984 00:00:23

0.9 Y 0.1 Sr Cr03 1 ATM Oxygen AF01 2R2

Data as Read by Doric DVM

0 -01850.00E6	1 +08542.00E-6	2 +08472.00E-6	3 +08431.00E-6
4 +08340.00E-6	5 Not Read	6 Not Read	7 Not Read
8 Not Read	9 -01010.00E-6	10 +02920.00E-6	11 +7779.00E-6
12 +11558.00E-6	13 +04858.00E-6	14 +08638.00E-6	15 +03779.00E06
16 Not Read	17 Not Read	18 Not Read	19 Not Read

T.C. Temp. (K) by Position: 1, 2, 3, 4 (4A, 3A, 7B, 8B; BNW 7838-ref. to NBC std.)
1 1347.8 1 1341.5 3 1329.3 4 1321.3 Ambient Temp. = 302.7
DeltaV(sample) = (- DeltaV (meas)) + S(Pt Leads)*Delta - t(*)

1 -0.00306340637112	2 -0.00819541690649	3 -0.0121505887325	4 -0.00513100890792
5 -0.00908717848862	6 -0.0039551673079		

S(PTSTDROD) = 2.238E-05 DeltaV(Pt) = -5.93E-04 Dtmax(K) = 26.48

Tavg1335.0	Abs. Seeorg2(6+0, 0)	4.49E-04 Volts/deg K	Origin-6.3E-05 volts
Tavg1335.0	Abs. Seebeck (6 PTS)	4.458E-04 volts/deg K	Origin-1.2E-04 volts
Tavg1335.0	Abs. Seeorg1 (thru 0, 0)	4.52E-04 volts/deg K	Origin 0.0E+00 volts

Dtmax(K) 26.5 Ori. error%: 1.0E+00 Sbeck; 5.3E-01 Sorg2
3 Sigmas: 1.4E-05Sbeck 1.5E-05 Sorg1 1.4E-05 Sorg2
% Seediff error -7.1E-01% Sbeck-Sorg2
Heating rate 0.0E+00 K/min
Expr. condition check: Rate, Dtt1&2, Ws1&2, Dtmas
Rate, DeltaT(max), Origins, 3 Sigma(seebeck&seeorg) are all within exper. limits

FIGURE B.7. Example of Seebeck Data Output

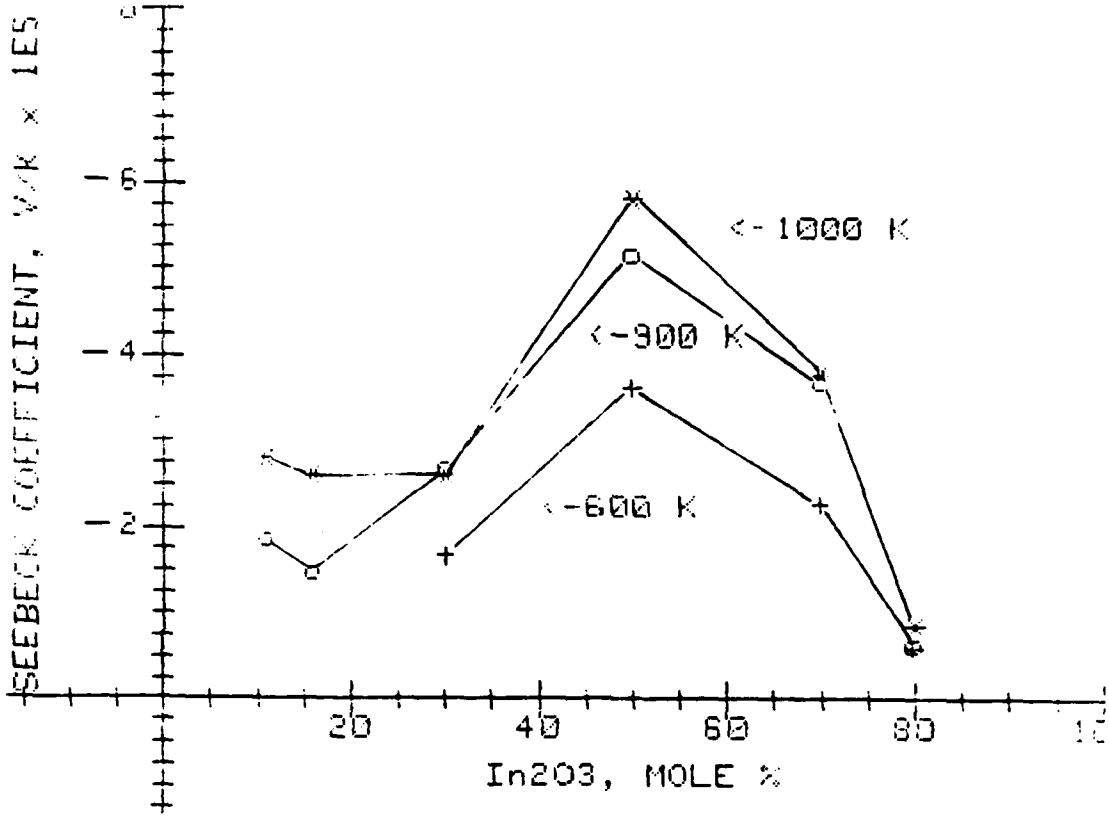

FIGURE B.8. Seebeck Cooefficient for SnO_2-In_2O_3

° Seebeck Apparatus

System Advantages

- Automated data acquisition, data analysis temperature cycle control

- Rapid (8 seond) data sampling allows data acquisition even during heating/cooling cycles (i.e. up to 2 degrees/minute) which results in Seebeck values within the 3 σ_s of ± 2.85% measured under thermal equilibrium conditions.

- Environmental pressure range: 10^{-4} torr to 2 atm

- Environmental atmosphere control: variable P_{O_2}
- Temperature range: 100°C to 1500°C

- Sample impedance: Limited to 10^4 Ohms or less.

END

FILMED

3-85

DTIC